AOE
Aerospace & Ocean Engineering
at Virginia Tech

FUSION AERONAUTICS
presents the
HB-86 NAVIGATOR

VirginiaTech
Invent the Future

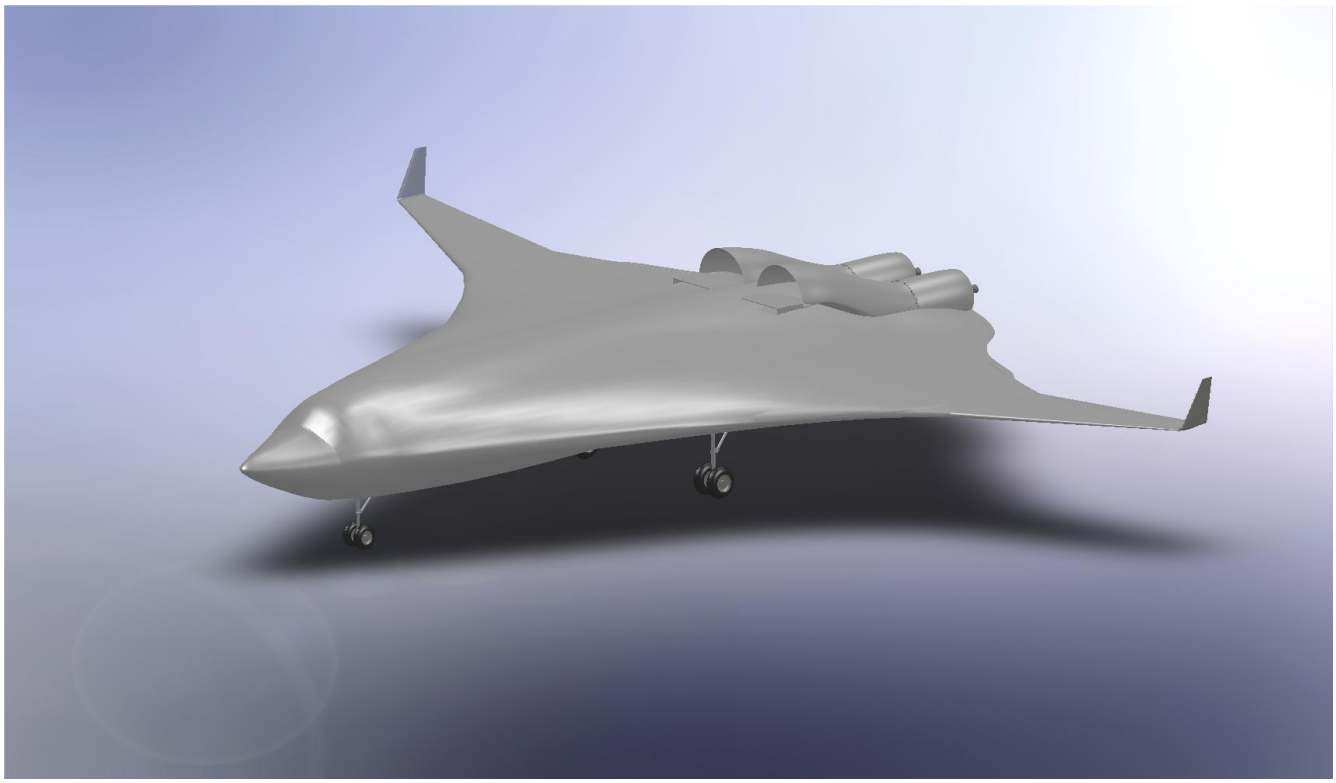

2008/2009 AIAA Undergraduate Team Aircraft Design

Member Roster

Name (Left to Right)	Position	AIAA #:	Signature
Joshuah Hess	Team Leader, Aerodynamics	**308983**	
Logan Thomas	Configuration	**262953**	
Robert Hill	Performance, Stability and Control	**308988**	
Rachel Van Buren	Propulsion and Noise	**309000**	
Subash Kafle	Weights, Sizing; Structures and Materials	**300758**	
Abhishek Naidu	Systems	**309354**	
Akash Patel	Cost	**309355**	

Dr. William H. Mason	Faculty Advisor	

Executive Summary

Fusion Aeronautics presents the *HB-86 Navigator* as a solution to the 2008-2009 AIAA Undergraduate Aircraft Design Competition RFP. The design will serve as a quiet, environmentally sound, subsonic, hybrid-wing body commercial transport to replace the Airbus 320 and Boeing 737. The main drivers for this proposal included maximizing performance capabilities with respect to the given RFP mission, while also maintaining a balanced, competitive commercial and environmental advantage. The requirements of the RFP are discussed later in Section 1.2.

Our innovative, hybrid wing aircraft is designed to replace existing medium-range commercial transports by the year 2018. With a low fuel burn and the use of a state-of-the-art geared turbofan, we have reduced operating cost while lowering our environmental impact. The integrated wing body provides for aerodynamic performance with low drag at cruise conditions. With the absence of a vertical tail, two clam-shell airbrakes are integrated with the winglets for any potential yaw disturbances. The cargo bay features a newly introduced design (an externally driven roller-pallet transport system) for cargo loading and retention, decreasing terminal turnaround time. Externally mounted cameras offer passengers unique views while also increasing in-flight safety. Another feature of the cabin is the high volume interior offering side compartments for storage in addition to overhead bins.

Table ES.1 tabulates key specifications of the *Navigator:*

Table ES.1: *Navigator* Specifications

Wingspan	140 ft.
Aspect Ratio	3.6
Overall Length	108 ft.
TOGW	145,000 lbs.
Maximum Thrust (sea level)	46,000 lbs.
Passengers	150 (dual class) 180 (single class)

The *Navigator* is a strong replacement for current subsonic, medium-range commercial transports. The combination of aircraft performance, capabilities, and competitive cost make our design a first-rate choice for future commercial transports. Table ES.2 details the *Navigator's* satisfaction of the AIAA RFP, while Figures ES.1, ES.2, and ES.3 are fold-outs detailing the configuration of the aircraft.

Table ES.2: RFP Compliance

Parameters	RFP	Navigator
Passenger Capacity	150 (dual class)	150 (dual class)
Cargo Capacity	7.5 ft^3/PAX	11.0 ft^3/PAX
Maximum Range	2800 nm	2873 nm
Initial Cruise Altitude	35,000 ft.	38,000 ft.
Community Noise	ICAO Chapter 4 – 20 dB	ICAO Chapter 4 – 20 dB
Fuel Burn	41 lbs/seat	41 lbs/seat
Operating Cost	8% reduction	8% reduction
Acquisition Cost	(~$ 36 billion for 1500 units on B737)	$32 billion for 1500 units

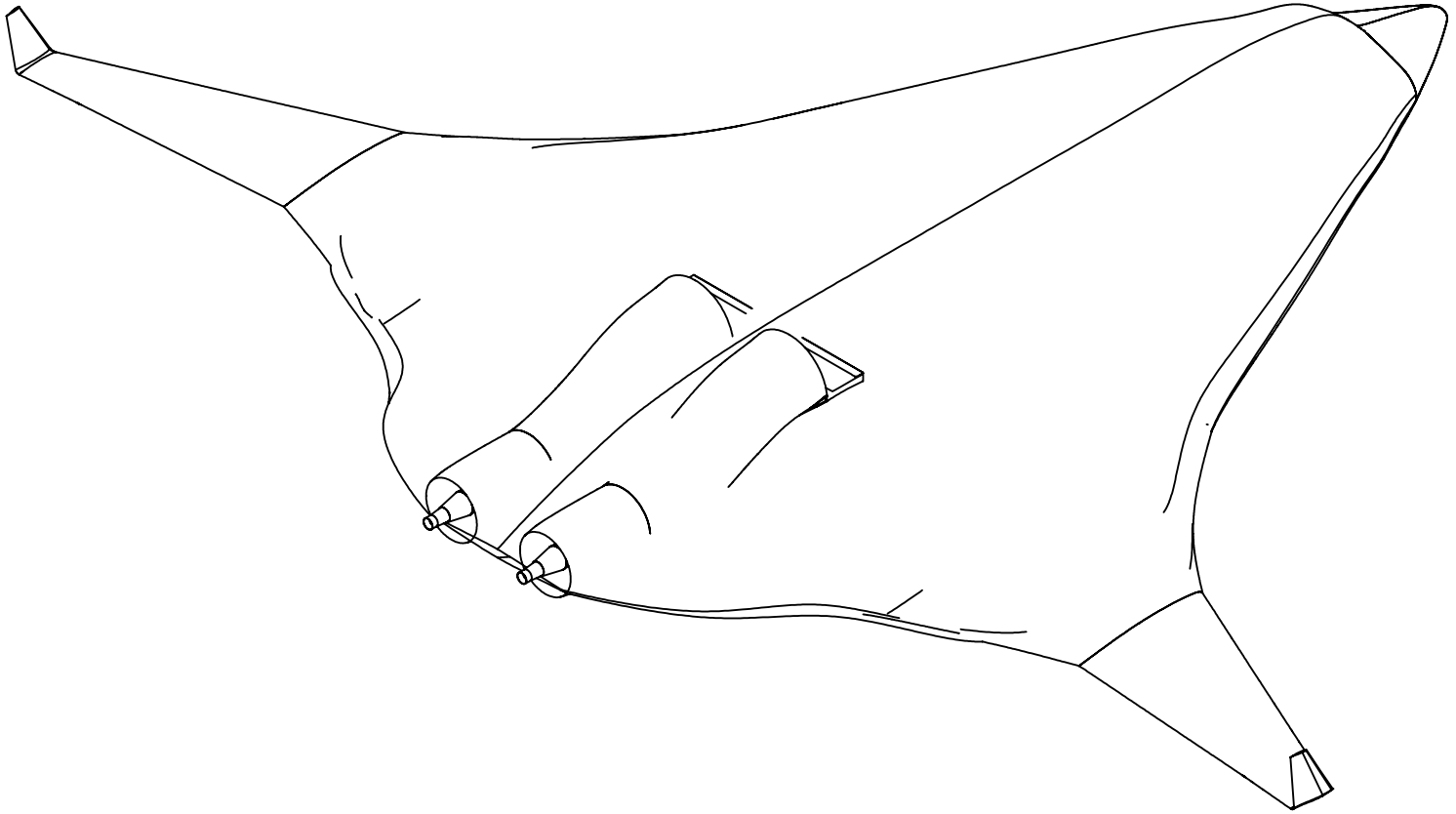

Figure ES. 1: Isometric Navigator View

	NAME	DATE	Fusion Aeronautics		
DRAWN	L. Thomas	5-11-09			
CHECKED	J. Hess	5-11-09	SIZE A	Navigator Isometric	REV.
			SCALE: 1:175		SHEET 1 OF 1

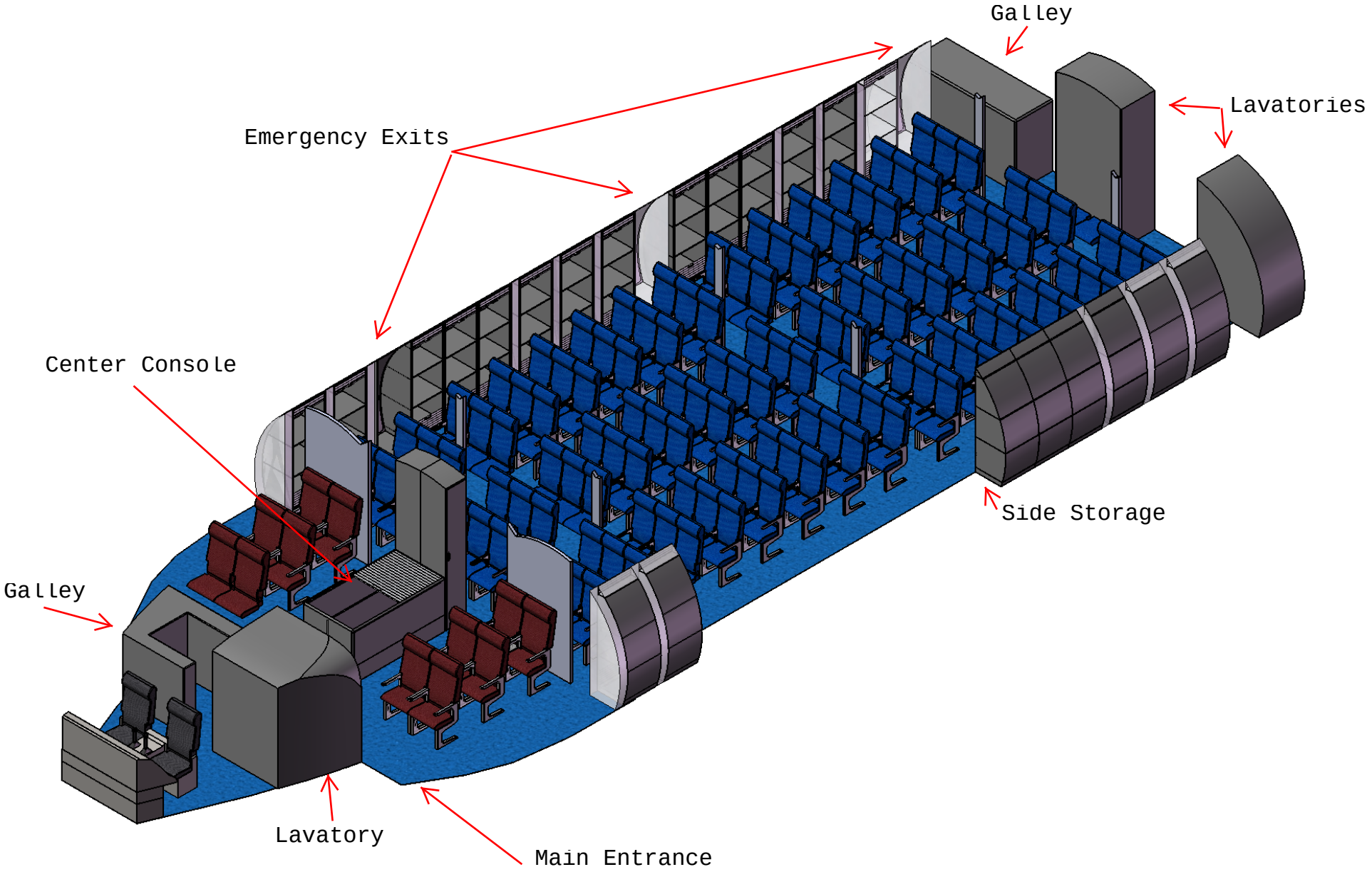

Figure ES.2: Isometric Cabin View

Fusion Aeronautics

	NAME	SIZE		REV.
DRAWN	Logan Thomas	A	Cabin Layout (Isometric)	
CHECKED	Joshuah Hess	SCALE:1:200	WEIGHT:	SHEET 1 OF 1

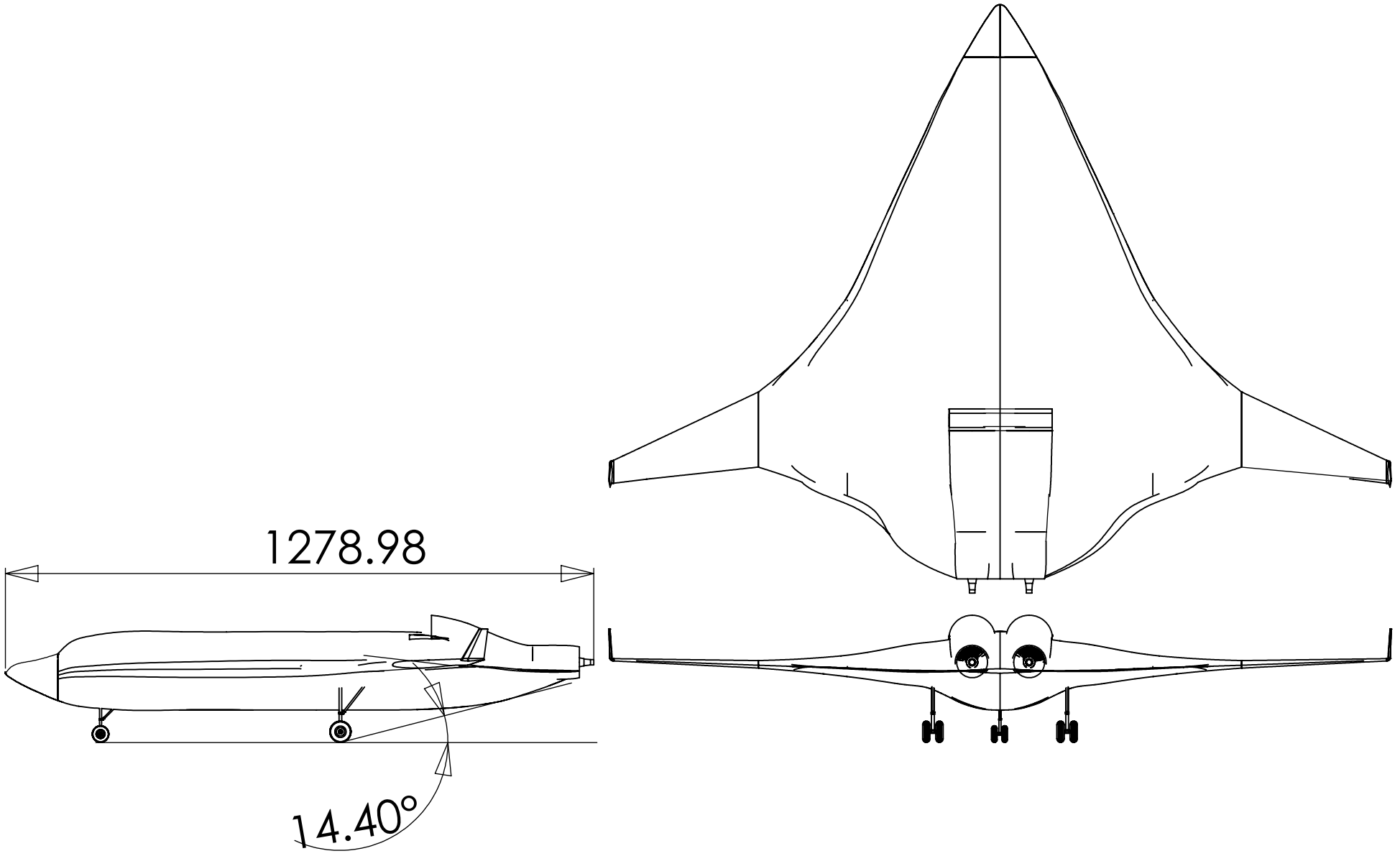

Figure ES. 3: Three View of HB-86

		NAME	DATE	
Dimensions in Inches	DRAWN	L. Thomas	5-11-09	Fusion Aeronautics
	CHECKED	J. Hess	5-11-09	
				A — Exterior 3-View — REV.
				SCALE: 1:300 — WEIGHT: 145,000 lb — SHEET 1 OF 1

Table of Contents

Title Page....1

Team Roster....2

Executive Summary....3

Table of Contents....8

Index of Tables, Figures, and Symbols....10

1. Introduction
    - 1.1 Background....13
    - 1.2 RFP Requirements....12
    - 1.3 Initial Design Selection....14
    - 1.4 Box-Wing Concept....15
    - 1.5 Three-Surface Concept....17
    - 1.6 Hybrid-Wing Concept....18
    - 1.7 Design Selection....19

2. Configuration and Layout
    - 2.1 Planform Selection....20
    - 2.2 Engine Configuration....21
    - 2.3 Cabin Design....23
    - 2.4 Emergency Exits....26

3. Sizing
    - 3.1 Mission Profile....27
    - 3.2 Mission Weight Fractions....27
    - 3.3 Sizing Constraint Diagram....30

4. Weights
    - 4.1 Weight Breakdown....31
    - 4.2 Center of Gravity Location....34

5. Propulsion and Noise
    - 5.1 Engine Selection....35
    - 5.2 Engine Specifications....36
    - 5.3 Engine Placement and Integration....37
    - 5.4 Engine Removal and Maintenance....38
    - 5.5 Noise....39

6. Performance
    - 6.1 Introduction....40
    - 6.2 Takeoff and Landing....41
    - 6.3 Climb and Descent....42
    - 6.4 Cruise....43

7. Aerodynamics
    - 7.1 Planform Design....44
    - 7.2 Airfoil Selection....45
    - 7.3 Drag Analysis....48

8. Stability and Control
8.1 General Issues 50
8.2 HB-86 Stability and Control Features 50

9. Structures
9.1 V-n Diagram 53
9.2 Structural Layout 53
9.3 Choice of Materials 57
9. 4 Stress Analysis 58
9.5 Finite Element Analysis 62

10. Systems
10.1 Landing Gear 64
10.2 Fuel System 65
10.3 Electrical System 66
10.4 Environmental Control/Lavatories and Gallies 67
10.5 Anti-Icing and Lightning Protection Systems 69
10.6 Avionics 69
10.7 In-Flight Entertainment 71
10.8 Passenger/Cargo Loading 72

11. Cost Analysis
11.1 Introduction to Cost Analysis 73
11.2 Initial Data 73
11.3 Cost of Research, Development, Technology, and Evaluation 74
11.4 Acquisition Cost 75
11.5 Flyaway Cost 76
11.6 Operating Cost 76

12. Conclusion 77

Index of Tables

Table ES.1: *Navigator* Specifications 3
Table ES.2: RFP Compliance 4
Table 1.1: Key RFP Requirements 13
Table 1.2: Comparative Aircraft Matrix 14
Table 1.3: Figure of Merit 19
Table 1.4: Figure of Merit Averages 20
Table 2.1: Geometric Characteristics Combinations 21
Table 3.1: Primary Mission Profile for *HB-86* 27
Table 3.2: Weight Fractions 28
Table 4.1: Initial Weight Breakdown of *HB-86 Navigator* 32
Table 4.2: Detail Components Weights and C.G. Locations 33
Table 5.1: Engine Comparison 35
Table 5.2: Calculate Engine Specifications 37
Table 6.1: *HB-86* Performance Results 41
Table 7.1: Parasitic Drag Component Breakdown 48
Table 8.1: JKayVLM Results 51
Table 9.1: Location of Pressure Bulkheads 57
Table 9.2: Stress Analysis for Wing/Fuselage Skin Panel 60
Table 9.3: Stress Analysis for Wing Spar 61
Table 9.4 Stress Analysis for Pressure Cabin Wall 61
Table 9.5: Stress Analysis for Longeron 62
Table 9.6: Material Yield Strength 62
Table 10.1: Landing Gear Data 64
Table 10.2: HB-86 Selected Tire Data 64
Table 10.3: Traditional and Untraditional Voltages 66
Table 11.1: Cost Factor Summary 74
Table 11.2: Break-Down of Research Cost 75
Table 11.3: Acquisition Cost 75
Table 11.4: Flyaway Cost in Millions 76
Table 11.5: Operating Cost in Billions Breakdown (*Navigator*) 76
Table 12.1: RFP Compliance 77

Index of Figures

Figure ES.1: Foldout of HB-*86* Isometric View 5
Figure ES.2: Foldout of *HB-86* Three View 6
Figure ES.3: Foldout of *HB-86* Cabin Configuration 7
Figure 1.1: Box Wing Three-View 15
Figure 1.2: Three-Surface Three-View 17
Figure 1.3: Hybrid-Wing Three-View 19
Figure 2.1: Right-View of *HB-86* 20
Figure 2.2: Wing-Sweep 21
Figure 2.3: Platypus Tail 22
Figure 2.4: Dual Class Layout 23
Figure 2.5: Console Diagram 24
Figure 2.6: Cabin Front View 24
Figure 2.7: Cabin Front Section View 25
Figure 2.8: Economy Class Storage Unit 25
Figure 3.1: Initial Sizing Plot 29
Figure 3.2: Weight Comparison 30
Figure 3.3: Thrust to Weight vs. Wing Loading Constraint Diagram 31

Figure 4.1: CG Range for *HB-86 Navigator* 34
Figure 4.2: CG Location for *HB-86 Navigator* 35
Figure 5.1: PurePower 1000G 36
Figure 5.2: Thrust Lapse 37
Figure 5.3: Inlet Geometry 38
Figure 5.4: Noise Certification Points 39
Figure 5.5: Current ICAO Noise Standards 40
Figure 6.1: Specific Range 43
Figure 7.1: Planform Geometry (Station Locations in Inches) 44
Figure 7.2: RAE(NPL) 5213 Plot 45
Figure 7.3: Lift Coefficient Verses Angle of Attack for RAE-5213 46
Figure 7.4: RAE-5213 Wind Tunnel Test Results 46
Figure 7.5: Pitch Moment Coefficient 47
Figure 7.6: Pressure Coefficient along Chord of RAE-5213 (M=0.78, α=0°) 47
Figure 7.7: Drag Polar for Takeoff, Landing (M=0.5, h = sea level) 49
Figure 7.8: Drag Polar for Cruise Conditions (M=0.8, h =40,000 ft) 49
Figure 9.1: V-n Diagram 52
Figure 9.2: Structural Layout of *HB-86* 55
Figure 9.3: Pressure Cabin Walls with Support Beams 56
Figure 9.4: Pressure Cabin Layout and Pressure Bulkheads Placement 56
Figure 9.5: Internal Structures Materials for the *Navigator* 58
Figure 9.6: Wing and Fuselage Skins Materials for *HB-86* 58
Figure 9.7: Elliptic Spanwise Loading 59
Figure 9.8: Spanwise Shear Distribution 59
Figure 9.9: Spanwise Bending Moment 60
Figure 9.10: Von Misses and URES Displacement Analysis for Wing Front Spar 63
Figure 9.11: Von Misses and URES Displacement Analysis for Wing Skin Panel 63
Figure 10.1: Electrical Brakes 65
Figure 10.2: Fuel Location 65
Figure 10.3: Electrical System Layout 67
Figure 10.4: Infrared Faucet 68
Figure 10.5: Lavatory Mirrors 68
Figure 10.6: Electro-Thermal Mats in Wings 69
Figure 10.7: Heads-Up Guidance Display 70
Figure 10.8: Boeing 787 Cockpit Layout 70
Figure 10.9: *Navigator* Cockpit Layout 71
Figure 10.10: In-Flight Entertainment System 71
Figure 10.11: Locations of Passenger and Cargo Loading 72
Figure 10.12: Cargo Layout 72
Figure 11.1: CEF Values from 1989 to 2008 74

Index of Symbols

Symbol	Definition	Units
AIAA	American Institute of Aeronautics and Astronautics	-
AR	Aspect Ratio	-
b	Wing Span	ft
BWB	Blended-Wing Body	-
c	Chord Length	ft, in
C_D	Airplane Drag Coefficient	-
C_{Do}	Airplane Zero-Lift Drag Coefficient	-
CG	Center of Gravity	-
C_L	Airplane Lift Coefficient	-

C_{lmax}	Maximum Airplane Lift Coefficient		-
D	Drag		-
deg	Degrees	-	
ft	Feet		-
hrs	Hours		-
kts	Knots		-
lb	Pounds		-
L	Lift		-
L/D	Lift Over Drag		-
LRC	Long Range Cruise		nm
MLW	Maximum Landing Weight		lb
MTOW	Maximum Takeoff Weight		lb
nmi	Nautical Miles		-
s	Seconds	-	
S	Airplane Wing Planform Area		ft^2
S_{VT}	Vertical Tail Area		ft^2
S_{HT}	Horizontal Tail Area		ft^2
SFC	Specific Fuel Consumption		lb/hp/hr
T	Thrust		lb
T/W	Thrust to Weight	-	
TOFL	Takeoff Field Length		nmi
TOGW	Takeoff Gross Weight		lb
V	Velocity		ft/s, kts
V_{stall}	Stall Velocity		ft/s, kts
V_{TO}	Takeoff Velocity		ft/s, kts
W	Weight		lb
W/S	Wing Loading		lb/ft^2
W_E	Empty Weight		lb
RFP	Request for Proposal		-
t/c	Thickness to Chord Ratio	-	
α	Angle of Attack		deg
ρ	Density		lb/ft^3

1. Introduction

1.1 Background

The RFP provided by the AIAA[1] is based upon a global commercial request for efficiency; this is with respect to both aircraft performance and environmental responsibility. Most evidently, economic demands have taken a toll on the commercial airliner industry. Environmental and economic pressures result in the request from the AIAA for a more environmentally sound, fuel efficient, ergonomic, and decreased noise commercial aircraft.

1.2 RFP Requirements

The RFP dictates specific requirements listed below in Table 1.1. In general, the RFP demands a commercial transport that is capable of carrying 150 passengers in a dual class configuration, with the capability of single-class adaptability in the same airframe. Cost plays a significant issue in the design of our aircraft by maintaining a comparative acquisition cost and a decreased operational cost. Several performance specifications in the RFP will constrain the design process (e.g., cruise Mach number, maximum range, etc.), as will the ability to be standardized to operate in current commercial airport infrastructure. Consider the following table for the RFP specifics:

Table 1.1: Key RFP Requirements

Cargo Capacity	>7.5 ft^3/passenger, bulk loaded
Maximum Payload Capability	Full single class 30” pitch passenger capacity (185 lbs/passenger) + full cargo hold (8 lbs/ft^3)
Maximum Landing Weight	Maximum Zero Fuel Weight (Reserves for Maximum Range (2800 nm) Mission)
Typical Mission Ranges	500 nm (50%), 1000 nm (40%), 2000 nm (10%)
Cruise Speed Requirement	0.78 Mach (LRC)
Takeoff Field Length	MTOW: 7000 ft. (sea level, 86°F)
Community Noise	ICAO Chapter 4 – 20 dB (cumulative)
Fuel Burn	< 41 lbs/seat [Objective: < 38 lbs/seat]

1.3 Initial Design Selection

To determine a baseline for our aircraft, a comparative aircraft study was found. Table 1.2 details the results of this study in a sample comparative aircraft matrix:

Table 1.2[2]: Comparative Aircraft Matrix

	Airbus A320	Boeing 737-700	All. Starliner 200	BD-700
Passengers	150-181	126-149	70	Bus. Jet NA
Hold Volume (ft^3)	1,369	1,002	N/A	N/A
Wing span (ft)	111	112	91	94
Wing Area (ft^2)	1,317	1,341	916	1,027
Wing Aspect ratio	9.39	9.4	9.2	8.6
0.25 Chord Sweep (deg)	25	25	Not Released	35
Length (ft)	123	110	86	99
Height (ft)	38	41	32	24
Tail span (ft)	40	47	35	31
Vertical tail area (ft^2)	231.4	284.2	Not Released	186
Horizontal tail area (ft^2)	333.7	353.1	Not Released	245
Number of Engines	2	2	2	2
Engines	IAE V2525-A5	CFM 56-7	BR700	BR710A-220
Static Thrust (lbs)	25,000	24,000	13,500	14,750
Empty weight (lbs)	92,113	84,100	44,700	50,300
Max T-O weight (lbs)	162,040	133,000	78,500	95,000
Max landing weight (lbs)	142,195	128,000	75,000	78,600
Max zero fuel weight (lbs)	134,480	120,500	Not Released	56,000
Max wing loading (lbs/ft^2)	123	98.85	86	92.95
Cruise Mach no.	0.84	0.785	0.84	0.85
Max Cruise altitude (ft)	37,000	41,000	Not Released	51,000
Design Range (nm)	2649	1540	2000	6010

From this table, a baseline for feasibility was developed for reference in our design. To satisfy the RFP, three initial concepts were evaluated with historical data using Table 1.2 as a reference. These three designs included a box-wing design, a three-surface configuration, and a hybrid wing-body design (the latter of which was chosen as our final design).

1.4 Box-Wing Concept

A possible design considered for study was a box-wing configuration. For a box-wing, the horizontal stabilizer at the tail of the aircraft is extended and joined to the wing; in effect, making the stabilizer a wing itself. This is different from a joined wing in that the wings are connected by a vertical endplate. This additional surface increases the overall span efficiency. However, the complexity of the design and few previously developed aircraft lead to many concerns. A three-view visualization of the box-wing design can be found below in Figure 1.1:

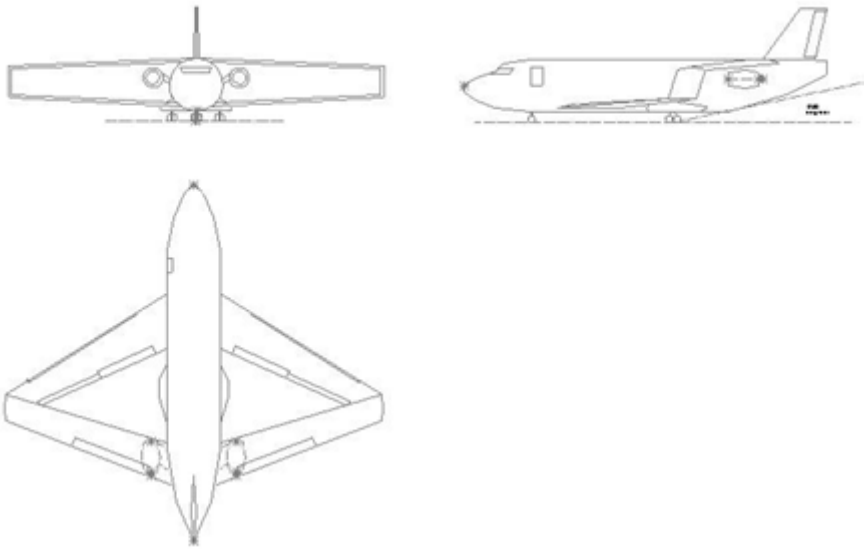

Figure 1.1: Box Wing Three-View

The key design features of the box-wing are predominately determined by the upper wing surface configuration. The lower wing must be swept back slightly for high speed flight at desired cruise speeds, while the upper wing must be swept forward in order to join the lower wing. This creates a tradeoff to be considered from aerodynamic, performance, and stability standpoints as the sweep of these wings and joint locations control important items such as cruise speed, center of lift, and pitching moment. Endplates between the two wings have been given the form of vertical winglets. In addition, the engines are located on the tail of the aircraft below the upper wing. This creates a thrust line as close to the lateral CG as possible, behind the rear bulkhead of the passenger compartment. For yaw control, a large vertical tail is required.

One of the potential problems with this configuration is that the aircraft wings will be under large stress due to bending moments at the endplates between the wings. These connections will require very careful planning and

shaping to ensure their stiffness to keep the aircraft stable. By having a completely separate upper wing, the total wetted area increases; in turn, increasing the skin friction. Because of strong viscous forces from the wings and the extra wing surface, another concern is the possible downwash and vortex interference. These issues make the configuration of the aircraft wings a stability and aerodynamic concern.

The development of a "family" of multiple aircraft would be a difficult task given the above concerns. For most airliners, a typical iteration in a family of aircraft simply means increasing the length of the aircraft by adding frames to the main fuselage; however, with the box-wing, this could inadvertently alter the aerodynamic characteristics of the aircraft. To solve this problem would require the development of an optimized configuration for the planned "family" instead of for the individual series—this severely limits future family expansion.

Fortunately, the very nature of the box-wing configuration offsets these disadvantages. By joining both the upper and lower wings, the wings themselves become a structurally stable frame. Through the increased planform area, much more lift is generated than a conventional wing design. This increase results in decreased take-off length, allowing for fuel-saving de-rated thrust takeoffs, decreased stall speeds, and a higher service ceiling. Lastly, from a ground crew prospective, the higher upper wing with engines mounted below allows for easy access to the engines during ground maintenance, and ensures the aircraft will be able to continue using existing facilities.

1.5 Three-Surface Concept

The three-surface concept was designed by considering two main characteristics: a higher lift to drag ratio (*L/D*) and additional control surfaces on the aircraft. The concept builds on conventional aircraft by adding a canard surface, as can be seen below in Figure 1.2:

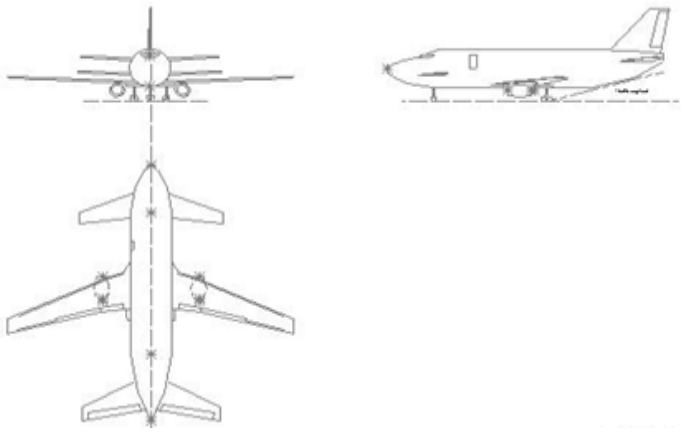

Figure 1.2: Three-Surface Three-View

The advantages of adding an extra surface or canard to an aircraft is increased lift at the nose region. This increase in lift yields a higher *L/D* ratio[3]. Similarly, the maximum lift coefficient can be increased by ten to fifteen percent.

When an aircraft encounters high gusts during cruise there is a sudden increase on the effective angle of attack, potentially resulting in a stalled wing. The canard is configured in such a way that the canard stalls before the actual wing. This provides the pilot enough time to react to the perturbation and recover. The three-surface design also has shorter take-off and landing distances. Another key advantage in the three-surface configuration is an increase in CG range.

However, the primary disadvantages include high skin friction, higher aircraft weight, and lower stability than the other two designs considered. The addition of the canard is a major contributor to an increase in skin friction. The canard weight increases the *TOGW* of the aircraft. Higher *TOGW* results in more fuel required for the mission. The addition of a canard has also been shown to move the aerodynamic neutral point forward in the aircraft, reducing the static margin.

1.6 Hybrid-Wing Concept

Recently, hybrid wing body designs have received increased attention as large capacity airliners. These airliners afford a much larger cabin volume than traditional tube and wing configurations of similar size. When applied to a smaller regional airliner, the increase in cabin space over a comparable tube-and-wing improves passenger comfort, boarding, and disembarkation. In addition a hybrid wing body configuration would have more volume for cargo. A hybrid wing body presents a cabin configuration radically different from aircraft currently in service. Multiple aisles could be used to allow more space for passengers to move within the cabin. Unused space could be used for a different means of storing carry-on items in lieu of overhead bins. This change would allow for an increase in both ease of movement and passenger comfort.

The hybrid wing body configuration offers a significant advantage in the area of noise reduction as well. While engine noise is not affected directly by aircraft configuration, airframe noise is due largely to the configuration of the wing, tail and high lift devices. As a hybrid wing body does not have a discrete fuselage, wing or tail, the noise normally produced in a tube-and-wing is not present. Hybrid wing configurations do not employ high lift devices, also eliminating a noise source[4]. This leads to a much cleaner wing and significantly reduced airframe noise. The hybrid wing body configuration also affords several aerodynamic and performance benefits. The maximum lift to drag ratio in a hybrid wing is approximately twenty percent higher than a comparable conventional aircraft[5]. This allows for lower fuel consumption during takeoff, and, consequently, reduced emissions.

The largest disadvantages of the hybrid wing concept appear in the areas of stability and structures. While a hybrid wing body configuration can be designed to be equally as stable as current aircraft, this requires compromising changes in terms of aerodynamic and performance advantages. Avoiding this loss, hybrid-wing bodies are typically designed to be much less stable than current airliners, but use flight computers for stability augmentation. The hybrid wing requires an unusual pressure vessel. Pressure vessels formed to non-cylindrical shapes are prone to failure. However, solutions to this problem have been proposed both for aircraft and non-body-of-revolution submarines.

With these advantages and disadvantages in mind the hybrid-wing-body concept was proposed. The conceptual configuration (as shown in Figure 1.3) would be of approximately the same wing span as a current Boeing 737, allowing it to operate in current airport facilities. The aircraft would carry the same number of passengers required in the RFP while organizing the cabin in such a way that passenger boarding and disembarkation processes would go more quickly and efficiently. Loading would also proceed at a more rapid rate.

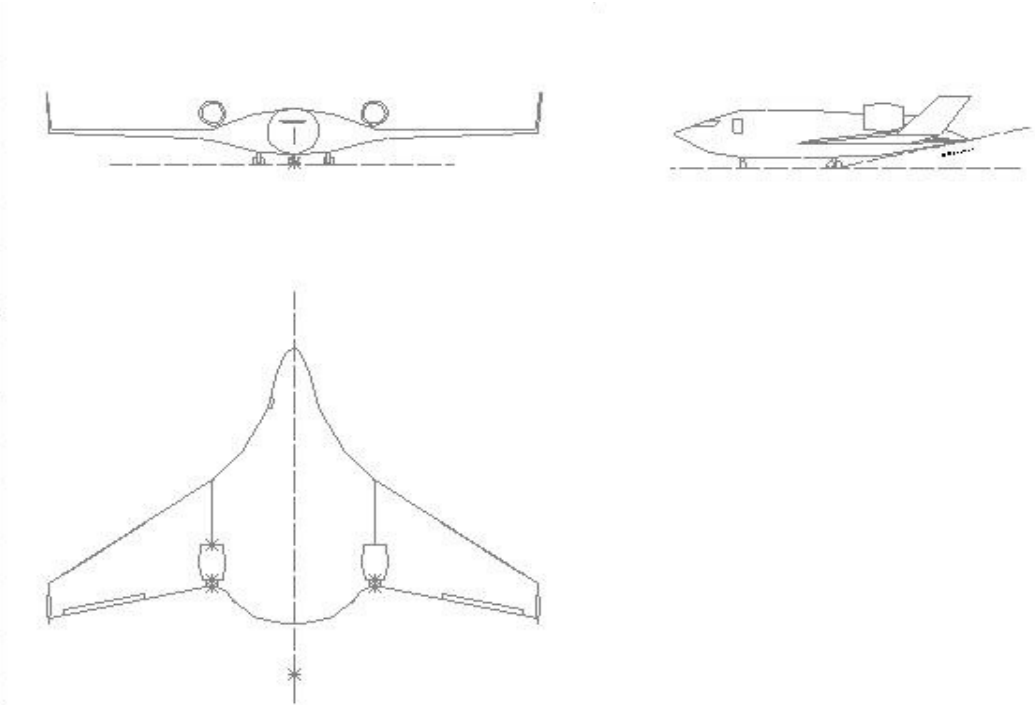

Figure 1.3: Hybrid-Wing-Body Three-View

1.7 Design Selection

The final design was decided by the use of the figure of merit from all team members. Each team member performed an individual analysis using previously mentioned baseline numbers and comparative aircraft studies. The Figure of Merit can be viewed in Table 1.3:

Table 1.3: Figure of Merit

Parameter	Parameter Weight
Noise	1
Cost	2
Weight	1.25
Performance Calculation	1
Ergonomics	1
Cargo Capacity	0.5
Fuel Burn	1.25
Infrastructure Operations	0.5
CG Sensitivity	1
Maintenance	1
Manufacturability	1.5
Cargo Loading Logistics	0.5
PAX Loading Logistics	0.5

Once the team members completed the concept matrix, the final results for each concept were averaged. Table 1.4 shows the ending result of each design.

Table 1.4: Figure of Merit Averages

Hybrid	Box	3SD
6.9443	6.9184	6.8668

The near equivalence of the averages indicates the value and precision that is inherent in each design. Although the hybrid wing body was the ideal concept, a reality check was performed to determine feasibility. The team considered everything from the amount of available data to the difficulty of designing such a concept. After careful consideration of pros and cons for each design, the final design was determined to be the hybrid wing body design.

2. Configuration and Layout

2.1 Planform Selection

The wing sections of the aircraft were chosen based on specific airfoils and performance characteristics that will be addressed in the aerodynamics section (Section 7). The pressure cabin required greater volume towards the center of the fuselage. This volume resulted in a non-airfoil cross section across the center 24.3percent of the wingspan. The center cross section was instead made a streamlined shape which would fit around the pressure cabin and blend smoothly into the airfoil cross sections of the wings without significantly increasing drag.

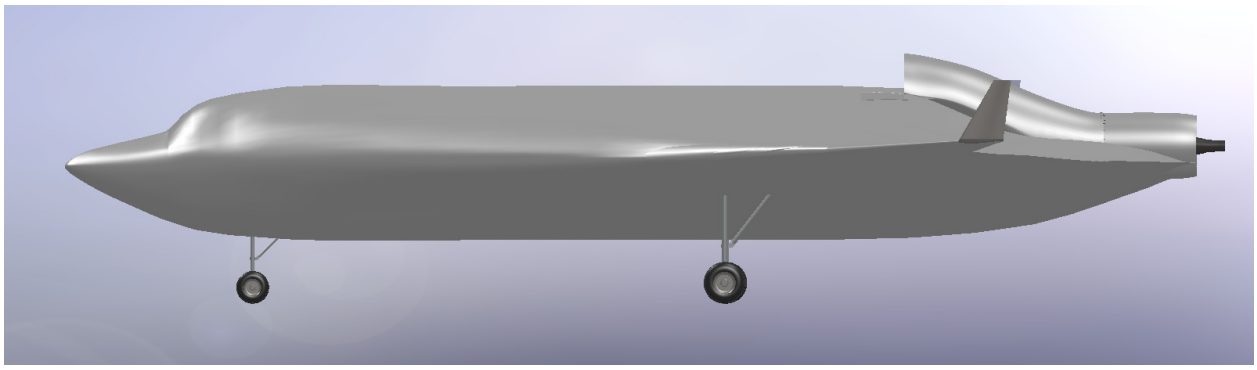

Figure 2.1: Right View of HB-86

Stability and control requirements largely dictated the top down geometry of the *Navigator*. In order to provide the necessary longitudinal stability, a considerable amount of wing sweep is required. Typically this value is between 30 and 40 degrees[6]. Using Figure 2.2[6] as a basis for an initial wing sweep at a cruise Mach number of 0.78, the team arrived at an initial estimate of 30 degrees.

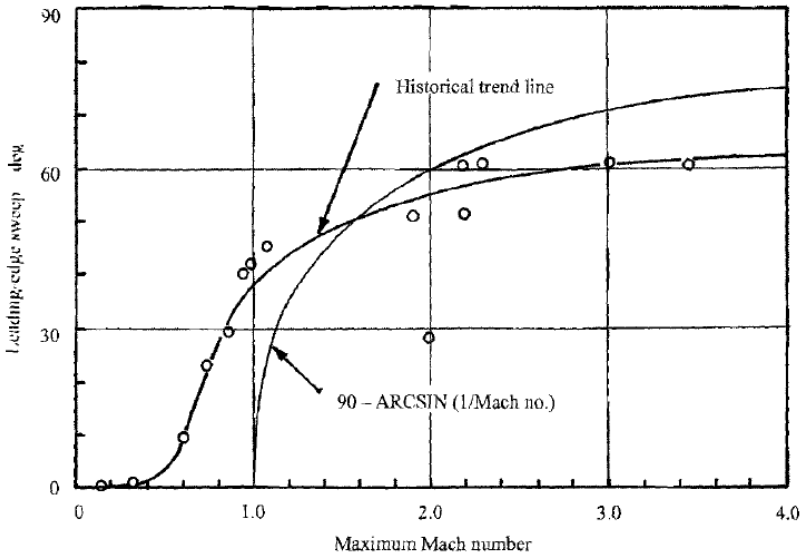

Figure 2.2: Wing Sweep[6]

RFP analysis placed an upper limit on the wing span of 150 feet. With these requirements, the team began varying the wing geometry to find a configuration that provided the necessary performance characteristics. The wing dimensions provided adequate space near the tip for the structure necessary to suppress twist. The center section was extended rearward in a "platypus tail" to provide a location for the semi-submerged engines.

2.2 Engine Configuration

Engine placement was driven primarily by engine out yaw control. Wing mounted engines place the thrust line of each individual engine a significant distance from the lateral center of gravity. Current commercial aircraft employ a large vertical tail on a large moment arm to balance the engine out induced moments. The hybrid wing body configuration does not allow for a long moment arm for the vertical tail. As such, a significantly larger vertical tail would be needed. In examining possible solutions to engine out control, the team realized that a vertical tail would

have to be so large that it would generate excess amounts of drag and additional weight. The option of two vertical stabilizers also led to the same conclusion. As hybrid wing body designs can operate safely and efficiently without a vertical tail, it was decided that the engines would be mounted as close to the center of gravity as possible.

Mounting the engine on pylons near the center of the aircraft on the upper surface would create significant structural problems, as well as difficulty for maintenance access. Pylon mounting on the lower surface created the same structural problems; although, while easier to access, this also raised the aircraft further above the ground. Hanging pylon-mounted engines encounter areas of poor airflow during take-off and landing. This location also raised the passenger loading door to a level inaccessible by a typical jetway. Pylon mounted engines above and below the aircraft also would subject the aircraft to strong pitching moments and a corresponding increase in trim drag.

Given these concerns, the engines were placed in a semi-submerged arrangement in the "platypus tail" on the upper surface of the aircraft as shown in Figure 2.3. This placed the thrust line of each engine laterally, 2.46 ft. from center of gravity, and 2.5 ft. above it. The resulting pitching moment is was minor, and split flaps on the winglets were sufficient to balance the yawing moment generated during engine out. This arrangement had the added benefit of providing easier maintenance access than the high mounted pylon design. For adequate airflow into the engines, S-ducts were used to ingest air from the upper surface and divert it into the engines. A boundary layer diverter was employed to reduce the thickness of the boundary layer entering the engine.

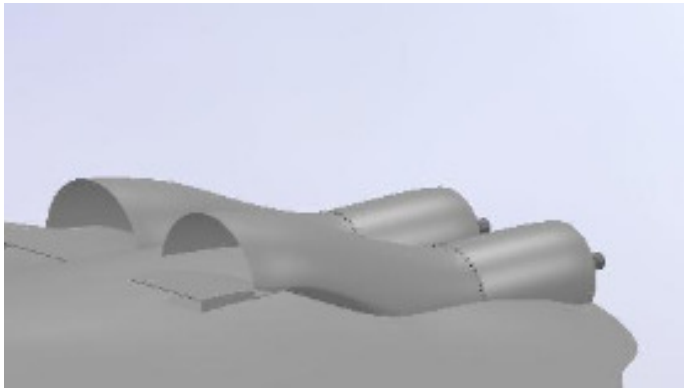

Figure 2.3: Platypus Tail

2.3 Cabin Design

One of the key elements of the *Navigator* was the improvement of passenger comfort and the reduction of loading times. While the hybrid-body design prohibits the installation of windows, the two class layout depicted in Figure 2.4 demonstrates the potential of this cabin design. The primary contributor to boarding time is "walking traffic" (backup that occurs as a result of passengers pausing to stow luggage); the cabin design of the *Navigator* avoids this dilemma:

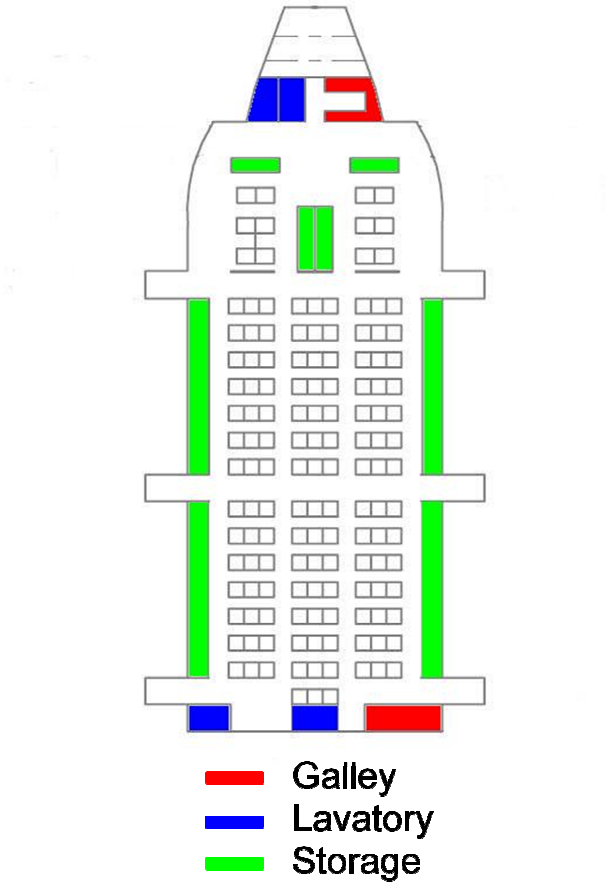

Figure 2.4: Dual Class Layout

Once through the main door passengers have access to three aisles in the first class section, which lead to four aisles in the economy section. The twenty-one inch wide aisles in the economy section are slightly larger than current aircraft.

First class seating is divided into two columns of seats with four seats in each of the three rows spaced 36 inches apart. Carry on storage for first class is located in a center console between the two columns of seats as shown in Figure 2.5. The storage unit is top loaded and divided in the center. The unit sits only 28 inches above the floor, allowing easy luggage access.

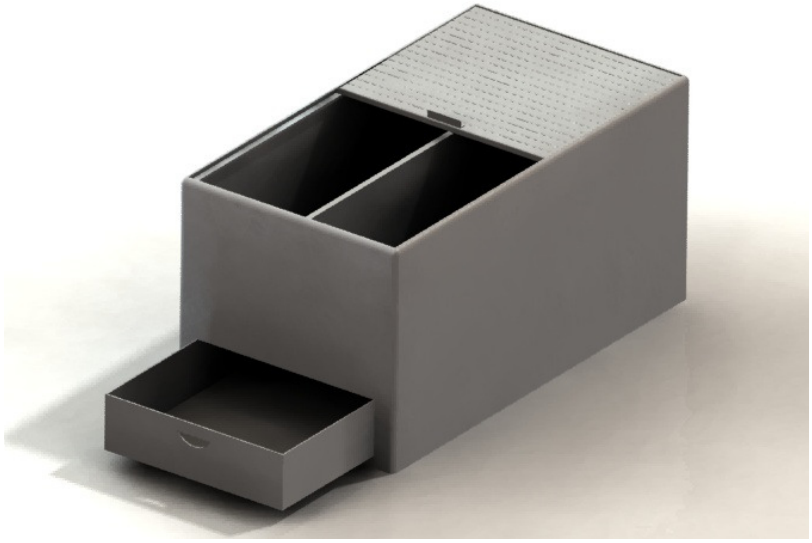

Figure 2.5: Console

Economy class is slightly less spacious. The seats are divided into three columns with nine seats per row spaced 32 inches apart. Seats are of comparable size to current aircraft with aisle widths being slightly larger. Storage for the center column of seats is located in overhead bins similar to current aircraft. The bin doors lower upon opening, allowing ease of access to luggage and plenty of headroom (Figure 2.6).

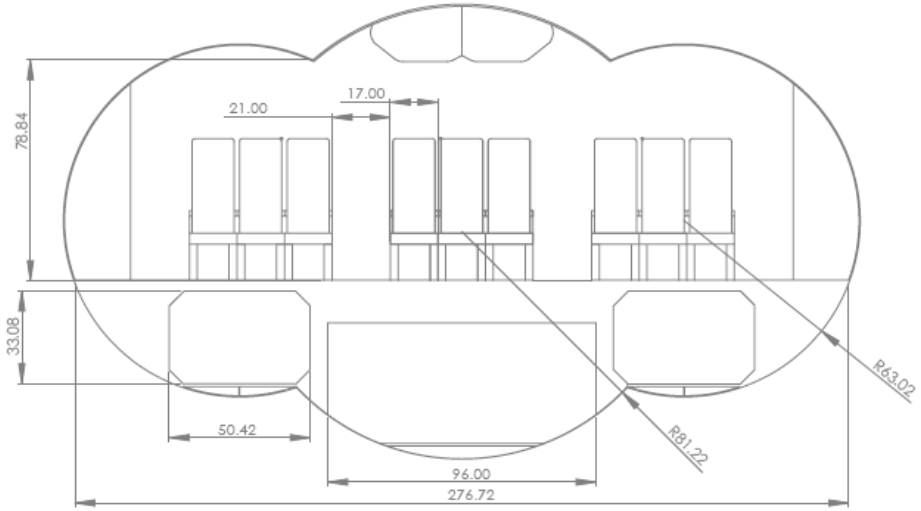

Figure 2.6: Cabin Front View

The cabin also contains three lavatories, one in the front of the cabin and two aft. A galley is also located in both the front and rear sections of the airplane. Figure 2.7 displays a front section view of the cabin, showing the braces not displayed in Figure 2.6. These braces are located on the edge of emergency exit rows in such a position that they do not interfere with seats or passenger movement towards the exits.

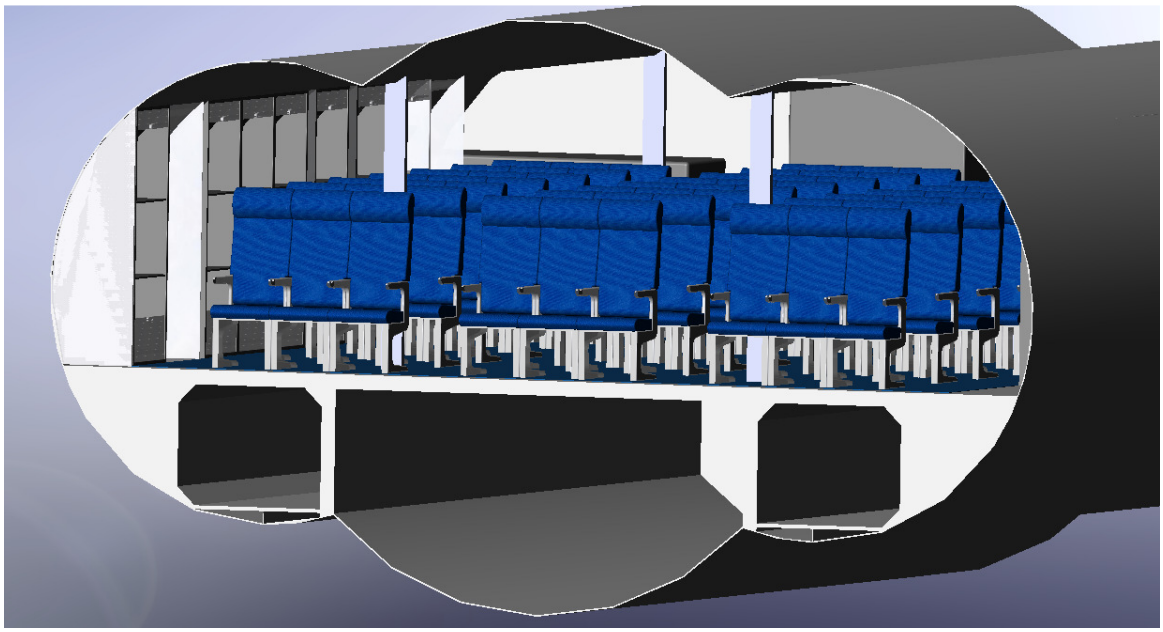

Figure 2.7: Cabin Front Section View

Storage for the outer columns of seats is located in closet-like storage units along the outermost aisles. These units have upward and downward retractable doors to prevent blocking the aisle, as seen in Figure 2.7.

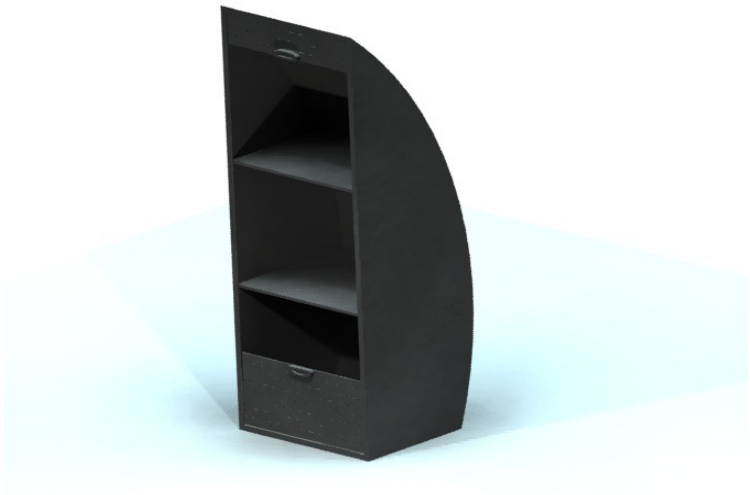

Figure 2.8: Economy Class Storage Unit

2.4 Emergency Exits

Two main entrances are located at the front of the first class section while an additional 6 emergency exits are spaced throughout the economy class section. The exit emergency doors to the pressure vessel are located at the ends of 24 inch wide exit aisles. Once through the pressure door, there is a three step staircase with handrails on either side leading to an exterior door. The staircase is short enough that a person with special needs may be pulled out in a safe manner. This section of the aircraft is not pressurized and the exterior door is lightweight and easily opened with a single latch release mechanism. If the latch will not release, a lever is placed adjacent to the door that when pulled will destructively remove the latching mechanism from the door. Passengers will exit to the area on top of the wing body towards the inflated ramp locations; ramps will also inflate at the front doors through which exit would be typical of a commercial transport. Figure 2.9 displays the exit procedure process:

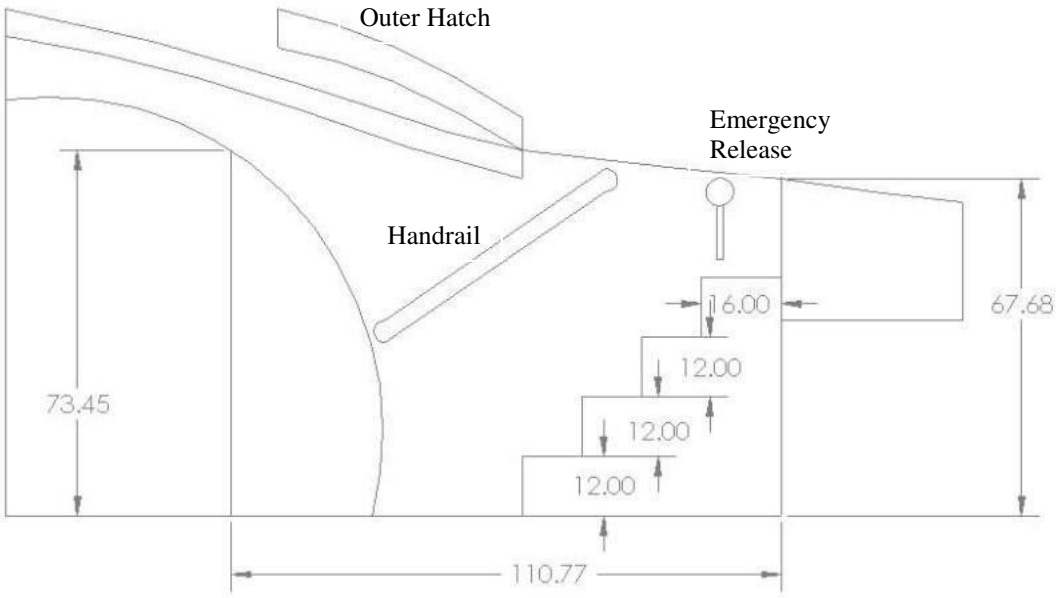

Figure 2.9: Emergency Exit Procedures

3. Sizing

3.1 Mission Profile

The mission profile that is called for in the RFP[1] is shown in Table 3.1 below:

Table 3.1: Primary Mission Profile for *HB-86*

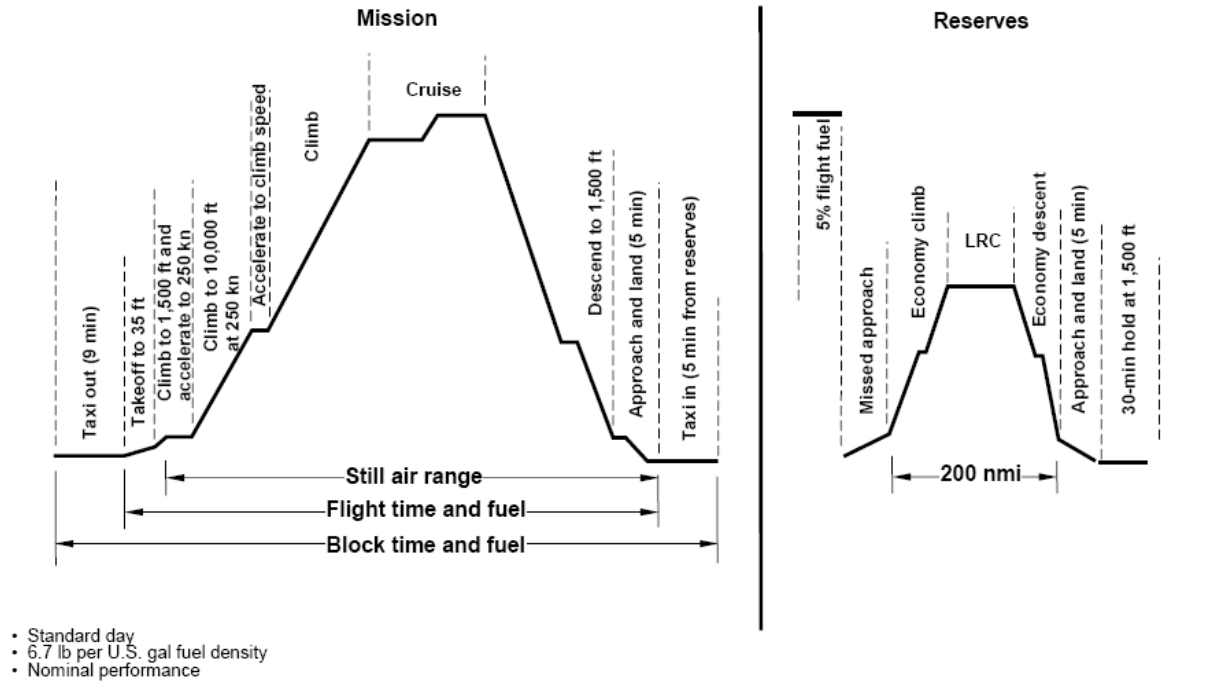

Mission Breakdown

- Take off at sea level with temperature of 86°F with takeoff field length of 7000 feet.
- Climb to cruise altitude
- Cruise at 35000 ft at Mach 0.78for 2800 nautical miles.
- Loiter for 30 minutes.
- Descend
- Landing at sea level

3.2 Mission Weight Fractions

The TOGW for the *Navigator* was calculated using an iterative process. The variables used and their values were the weight fractions for different mission profile segments, lift to drag ratio (*L/D*) of approximately 20, maximum lift coefficient of 1.6, cruise specific fuel consumption of 0.53, loiter sfc of 0.29. Predefined variables, such as weight

fractions for takeoff, climb, and landing, were obtained from Roskum[7] and Raymer[6] and can be seen in Table 3.2 below. The weight fractions for cruise and loiter were calculated using the following equations.

$$\left(\frac{W_e}{W_o}\right)_{cruise} = e^{\left(\frac{-Range \cdot sfc_{cruise}}{V_{cruise} \cdot \frac{L}{D}}\right)} \tag{3.1}$$

$$\left(\frac{W_e}{W_o}\right)_{loiter} = e^{\left(\frac{-E \cdot sfc_{loiter}}{\frac{L}{D}}\right)} \tag{3.2}$$

The weight fractions used for the takeoff, climb, and landing segments were 0.9700, 0.9850 and 0.9950 respectively. Using the above equations, the calculated values for weight fractions for cruise and loiter were 0.8547 and 0.9928, respectively. The total weight fraction was calculated by taking a product of all the segment weight fractions.

$$\left(\frac{W_e}{W_o}\right)_{final} = \left(\frac{W_e}{W_o}\right)_{takeoff} \left(\frac{W_e}{W_o}\right)_{climb} \left(\frac{W_e}{W_o}\right)_{cruise} \left(\frac{W_e}{W_o}\right)_{loiter} \left(\frac{W_e}{W_o}\right)_{landing} \tag{3.3}$$

$$\left(\frac{W_e}{W_o}\right)_{fuel} = \left(1 + \frac{trapped\ fuel\ \%}{100}\right) \cdot \left(1 - \left(\frac{W_e}{W_o}\right)_{final}\right) \tag{3.4}$$

The calculated total fuel fraction for the mission is 0.2127. Table 3.2 lists all the weight fractions:

Table 3.2: Weight Fractions

Mission Segment	**Weight Fractions (*We/Wo*)**
Takeoff	0.9700
Climb	0.9850
Cruise	0.8547
Loiter	0.9928
Landing	0.9950
Total Weight Fractions	**0.8067**
Total Fuel Fraction	**0.2127**

Using the above weight fractions the initial TOGW and the initial empty weight (W_E) for the *Navigator* were calculated as seen in Figure 3.1. The initial estimates were calculated using baselines from *Boeing 737* and *Airbus A320*.

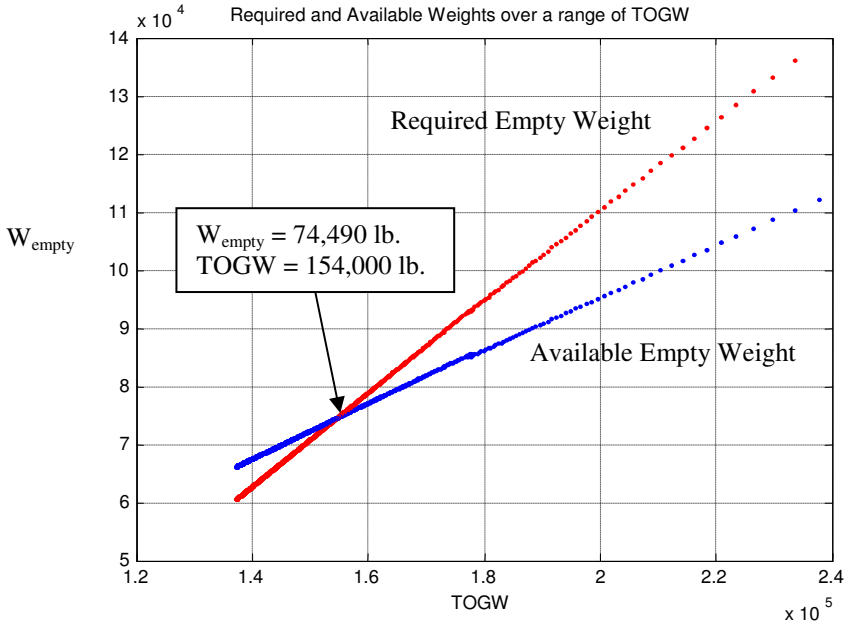

Figure 3.1: Initial Sizing Plot

The following equations were used from Raymer[5] to calculate the takeoff gross and empty weights:

$$TOGW = \frac{W_{fixed}}{1-\left(\frac{W_e}{W_o}\right)_{fuel}-\left(\frac{W_e}{W_o}\right)_{empty}} \tag{3.5}$$

$$\left(\frac{W_e}{W_o}\right)_{empty\ available} = TOGW - TOGW \cdot \left(\frac{W_e}{W_o}\right)_{fuel} - Weight_{fixed} \tag{3.6}$$

$$\left(\frac{W_e}{W_o}\right)_{empty\ required} = 0.911 \cdot TOGW^{0.947} \tag{3.7}$$

The initial takeoff gross weight and empty weight were 154,000 lbs and 74,490 lbs. After several iterations, the final takeoff gross weight was determined to be 145,000 lbs with empty weight of 67,000 lbs. The total fuel weight for the mission is 34,200 lbs. Figure 3.2 shows a comparison between current aircraft and the *Navigator*. As can be seen, the *HB-86* offers ten to fifteen percent weight TOGW savings and twenty to thirty percent empty weight savings.

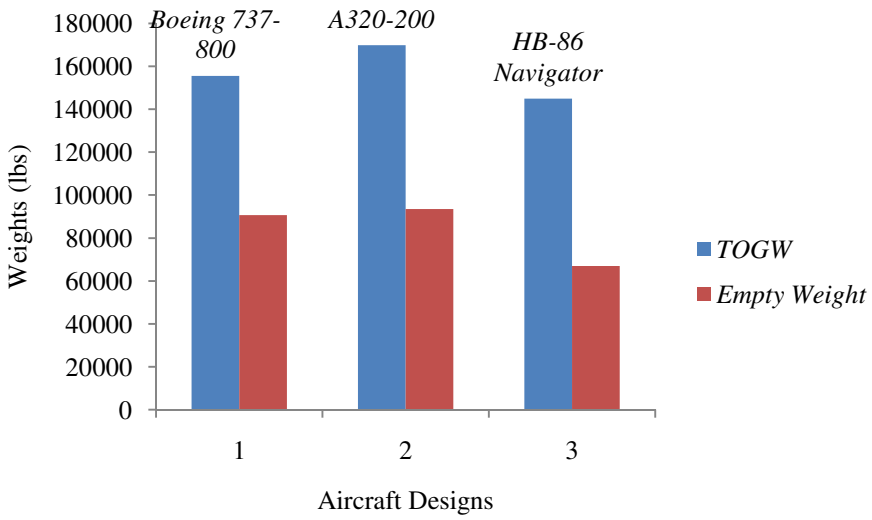

Figure 3.2: Weight Comparison

3.3 Sizing Constraint Diagram

Once the final TOGW and empty weight were calculated for the *Navigator*, the design wing loading (*W/S*) and thrust to weight ratio (*T/W*) were calculated using following relations from Raymer[5] and Mason[7].

$$\left(\frac{T}{W}\right)_{takeoff} = \frac{37.7 \cdot \frac{W}{S}}{\sigma \cdot CL_{max_{takeoff}} \cdot Takeofflength} \tag{3.8}$$

$$\left(\frac{T}{W}\right)_{cruise} = \left(\frac{q \cdot Cd_o}{\frac{W}{S}}\right) + \left(\frac{\frac{W}{S}}{q \cdot \pi \cdot AR \cdot e}\right) \tag{3.9}$$

$$\left(\frac{T}{W}\right)_{cruise_{sea\ level}} = \frac{\left(\frac{T}{W}\right)_{cruise}}{\left(\left(\frac{W_e}{W_o}\right)_{takeoff} \cdot \left(\frac{W_e}{W_o}\right)_{climb}\right) \cdot \left(\frac{Thrust_{takeoff}}{Thrust_{cruise}}\right)} \tag{3.10}$$

$$\left(\frac{W}{S}\right)_{landing} = \left(\frac{Landing\ Speed}{17.15}\right)^2 \cdot \sigma \cdot Cl_{approach} \tag{3.11}$$

$$\left(\frac{T}{W}\right)_{segment\ climb} = \left(\frac{number\ of\ engines}{number\ of\ engines - 1}\right) \cdot \left(climb\ gradient + \frac{1}{\left(\frac{L}{D}\right)_{segment}}\right) \quad (3.12)$$

The initial calculated values for *T/W* and *W/S* were 0.2215 and 116 lb/ft^2 respectively, which were similar in magnitude to the *Boeing 737* and *Airbus A320*. After further work it was found that hybrid body configurations have lower wing loadings compared to conventional aircraft[8]. Noted in Figure 3.3 below, the final wing loading (*W/S*) for the *Navigator* is 76 lb/ft^2 and a thrust to weight ratio of 0.2411.

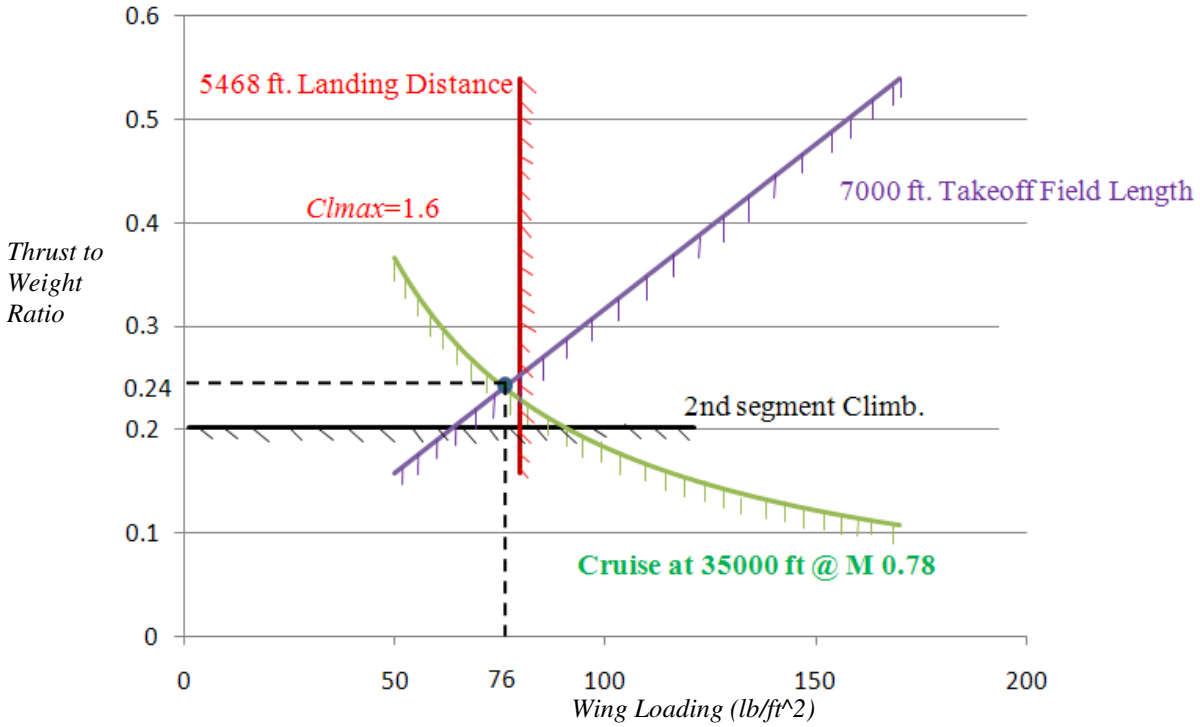

Figure 3.3: Thrust to Weight vs. Wing Loading Constraint Diagram

4. Weights

4.1 Weight Breakdown

The initial weight breakdown was based on Raymer[5] and can be seen in Table 4.1. The weights of the payload, crew and cargo weights are specified in the RFP[1].

Table 4.1: Initial Weight Breakdown of *HB-86 Navigator*

Weight Distribution (lbs)	
Cargo weight=1125 ft^3×(8lbs/ft^3)	8,700
Crew weight (Assuming number of crews-6 @ 225lb/crew)	1,350
Passenger weight (150 passenger @ 225 lbs/passenger)	33,750
Fuel weight (for 2800nm range)(includes 10% trapped and reserve fuel)	34,200
Empty Weight	67,000
Total Take Off Gross Weight	**145,000**

The various components involved in the weight breakdown include the wing, fuselage, nacelles, landing gear, propulsion, and fixed equipment. The detailed empty weight breakdown of *HB-86 Navigator* was based on Raymer[5] and Roskam[9]. Component weights were calculated for our designs; however, values for standard equipment were used based on available data[10]. The detail weight breakdown table can be seen in Table 4.2 below:

Table 4.2: Detail Components Weights and C.G. Locations

Components	weight (lbs)	X c.g (ft)	Z c.g.(ft)	Moment ft-lb (WiXi)	Moment ft-lb (ZiXi)
Structures					
Wing	13680.28	69.94	1.67	956855.97	22800.46
Fuselage	17150.00	48.41	0.00	830231.50	0.00
Main Landing Gear	4934.72	64.67	-6.22	319150.24	-30704.93
Nose Landing Gear	695.26	19.00	-6.22	13212.03	-4326.04
Engine Mounts (Nacelle)	3069.72	90.22	4.67	276964.99	14325.37
Structures Weight	**39529.98**	**60.62**	**0.05**	**2396414.74**	**2094.85**
Propulsion					
Engine (s)-installed	10000.00	90.22	4.67	902248.06	46666.67
Engine controls	10.00	90.22	6.22	902.25	62.22
Starter	248.73	90.22	4.67	22441.92	1160.76
Fuel system/tanks	151.27	66.75	-0.31	10097.13	-47.06
Propulsion Weight	**10410.00**	**89.88**	**4.60**	**935689.36**	**47842.58**
Equipments					
Flight controls	1766.41	58.29	-1.56	102958.53	-2747.75
APU	1885.00	80.64	1.56	152012.83	2932.22
Instruments	370.59	10.38	-1.56	3846.66	-576.47
Hydraulics	1305.00	64.67	-1.56	84400.12	-2030.00
Electrical	1564.92	48.71	6.22	76220.02	9737.27
Avionics	1646.64	10.38	-1.56	17091.85	-2561.44
Furnishings	6041.31	47.33	1.56	285947.86	9397.59
Air Conditioning	1405.83	67.87	-1.56	95411.14	-2186.85
Anti-icing	290.00	90.22	1.67	26165.19	483.33
Load and Handling	95.20	47.33	-1.56	4505.85	-148.08
Equipments Weight	**16370.89**	**51.83**	**0.75**	**848560.06**	**12299.83**
Total Empty Weight	**66310.87**	**63.05**	**0.94**	**4180664.16**	**62237.27**
Useful Load					
Crew flight deck	450.00	9.42	3.11	4239.77	1400.00
Cabin attn front	450.00	23.16	1.56	10419.77	700.00
Cabin attn rear	450.00	72.66	1.56	32696.51	700.00
Fuel	34200.00	66.75	-0.31	2282863.26	-10640.00
Passengers	33750.00	46.55	1.56	1571049.42	52500.00
Cargo/Payload	8700.00	46.55	-3.11	404981.63	-27066.67
Misc useful load	690.00	93.26	-3.11	64348.65	-2146.67
Total Useful Weight	**78690.00**	**55.54**	**0.20**	**4370599.00**	**15446.67**
Total TOGW	**145000.87**	**58.97**	**0.54**	**8551263.16**	**77683.93**

4.2 Center of Gravity Location

The center of gravity for the *Navigator* was calculated as seen in Table 4.2. The equation used was

$$X_{C.G.} = \frac{\sum w_i x_i}{w_i} \tag{4.1}$$

The calculated CG location for a TOGW of 145,000 lbs is 58.97 ft from the nose of the aircraft and 0.54 ft above the centerline as can be seen in Figure 4.2. Different loading conditions were also analyzed for *HB-86 Navigator* and corresponding CG locations were calculated. The calculated percentage of CG travel for *HB-86 Navigator* is 14.9 percent. Figure 4.1 shows the different weight conditions and their corresponding CG locations.

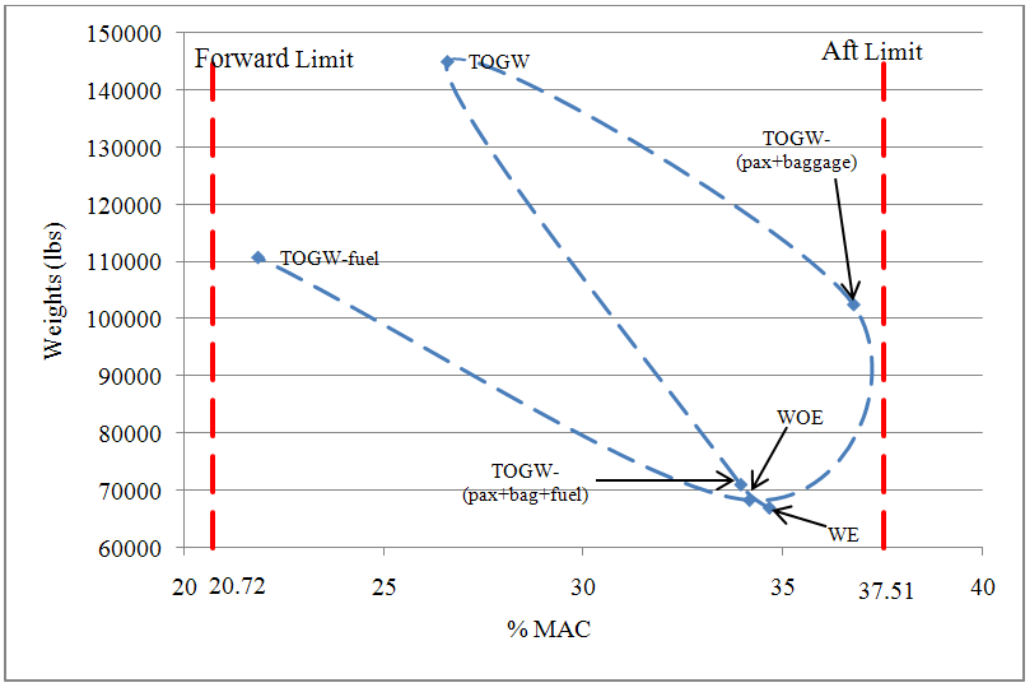

Figure 4.1: *CG* range for *HB-86 Navigator*

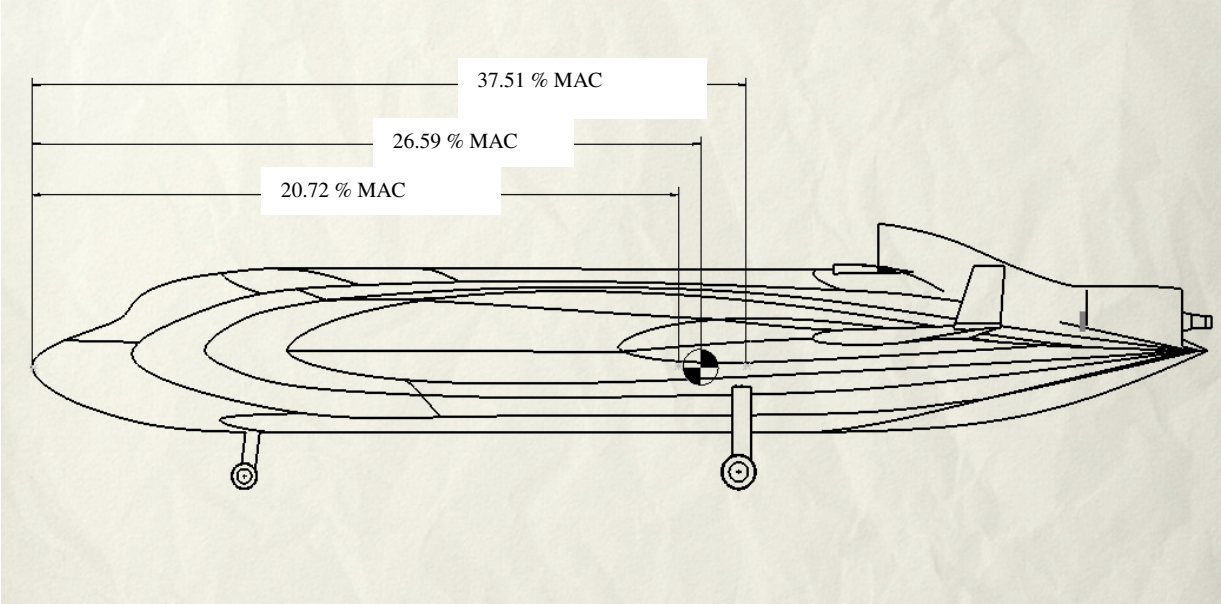

Figure 4.2: CG location for *HB-86 Navigator*

5. Propulsion and Noise

5.1 Engine Selection

Three main categories of engines were available to choose from for the propulsion system: turbojet, turbofan, and turboprop. A turbojet is designed for performance which results in a noisy engine with poor fuel economy. Such an engine would not help us meet the RFP requirements. The external blades of a turboprop engine create significant noise and do not operate at our required cruise speed of 0.78 Mach. The integration of an engine with external blades into our design would also provide a significant design challenge. Therefore, it was decided to use a turbofan for powering the aircraft. Looking more closely at the turbofan family, three engines were compared. Based on the preliminary weight estimates, a range of thrusts between 21,000 and 28,000 lbs. was used to narrow the selection. Table 5.1 below shows the engines and some of their basic characteristics:

Table 5.1: Engine Comparison

Engine	**CFM56-7B27** [11]	**V2500** [12]	**PW1000G** [13]
Dry Thrust (lb)	27,300	25,000	23,000
SFC	0.38	0.35	-12% (vs. current)
Bypass Ratio	5.1	5.4	-
Length (in)	98.7	126	-
Fan Diameter (in)	61.0	63.5	73
Weight (lb)	5216	5074	Less than current

Based on the specifications of the above engines, the one chosen for the *Navigator* was the Pratt and Whitney PurePower 1000G, seen in Figure 5.1 below. Although little technical data is available for this engine, Pratt and Whitney have promised lower fuel consumption, lower emissions, and lower weight than their current engines of the same thrust rating. They also expect to reduce engine noise by 20 dB[13]. The most unique feature of the engine is the gearbox, which allows the fan and low pressure turbine to operate at their individual optimum speeds. The lower fan speed will decrease noise, and advanced, lightweight materials will decrease engine weight. The engine is projected to be available by 2013, allowing our aircraft to enter service in 2018.

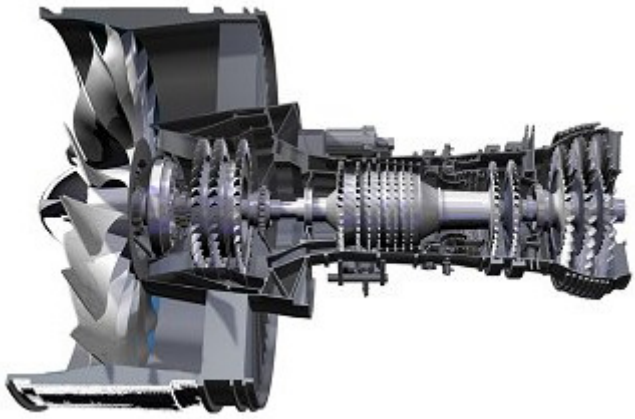

Figure 5.1: PurePower 1000G[14]

5.2 Engine Specifications

Since the PW1000G is still under development, there exists a minimal amount of technical data. Therefore, various equations and scaling techniques, described below, were used to estimate engine characteristics. First, cruise thrust was determined by creating a thrust lapse plot (Figure 5.2). The values calculated are maximum thrust values at altitude. To obtain a value for cruise, 85 percent of the max thrust was used as the cruise setting. This resulted in an estimated thrust of 5,300 lbs at a cruise altitude of 38,000 ft. Next, an SFC value was calculated. Pratt and Whitney have indicated a 12 percent reduction in fuel burn from current engines. The SFC of the CFM56-7B27 was used as the comparison. Subtracting 12 percent resulted in estimated dry and cruise SFCs of 0.29 and 0.53 respectively. Table 5.2 lists these and other calculated values for the engine.

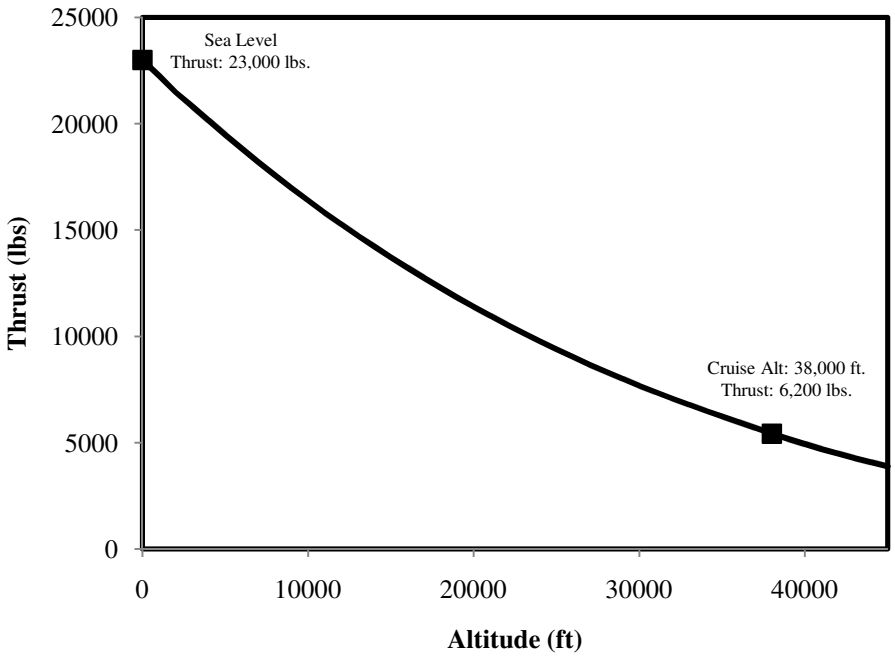

Figure 5.2: Thrust Lapse

Table 5.2: Calculate Engine Specifications

Cruise Thrust (lb)	5,300
SFC dry	0.29
SFC cruise	0.53
Mass Flow (lb/s)	962

5.3 Engine Placement and Integration

To reduce ground noise, the engines were placed on top of the aircraft. The engines are located near the centerline to avoid a large yawing moment in case of an engine-out situation. It was also decided to partially submerge the engine and intake. In contrast to pylons, submerging the engines creates a cleaner top surface of the aircraft. The inlet design is shown in Figure 5.3:

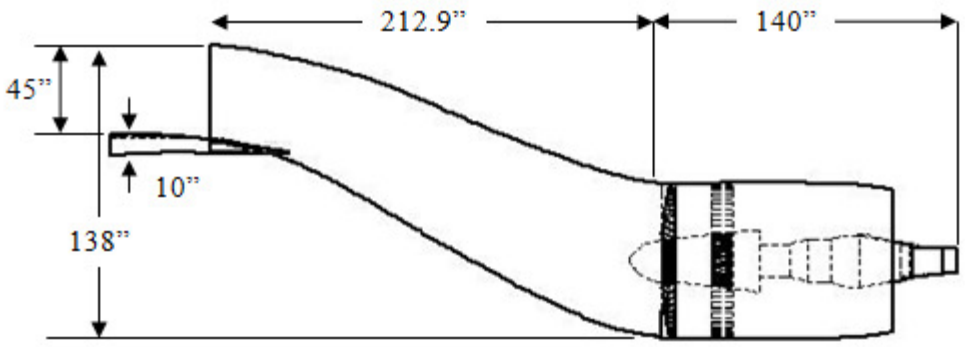

Figure 5.3: Inlet Geometry

To design the inlet, a few considerations had to be taken into account. First, the area of the intake had to be calculated. Using a mass flow rate of 962 lb/s (estimated from fan diameter[5]), the capture area was calculated to be 24.05 ft.^{2}. Therefore, the inlet area had to be sufficiently large to allow the correct amount of airflow into the engine. Secondly, the quality of the flow into the engine had to be maintained. A boundary layer diverter, similar to one used for the B-2 stealth bomber, diverts the boundary layer away from the engine. Air flow control also includes the air as it moves through the duct. This is achieved through vanes located inside the duct to control vortices created by the bend in the inlet.

5.4 Engine Removal and Maintenance

The engines are mounted on the top rear of the aircraft, which is unconventional for most current planes. To remove the engines from the top would require a special crane or hoisting equipment. Having them drop through the bottom of the aircraft was another possibility considered; however, the structural layout would be difficult. Therefore, it was decided to remove the engines from the rear of the aircraft. A lift and pulley system will allow the engine to slide out of its housing and be lowered to the ground. Pratt and Whitney have stated that the PW1000G will have fewer parts than competitive engines. They also use more durable materials, decreasing the number of scheduled maintenance checks. These two factors contribute to a lower maintenance time and cost.

5.5 Noise

The RFP requires a cumulative noise reduction of 20 dB relative to current standards. All aircraft must meet the International Civil Aviation Organization's (ICAO) noise requirements. The requirements can be found in Annex 16- *Environmental Protection*, Volume I- *Aircraft Noise*. The noise certification points are given in Figure 5.4 below:

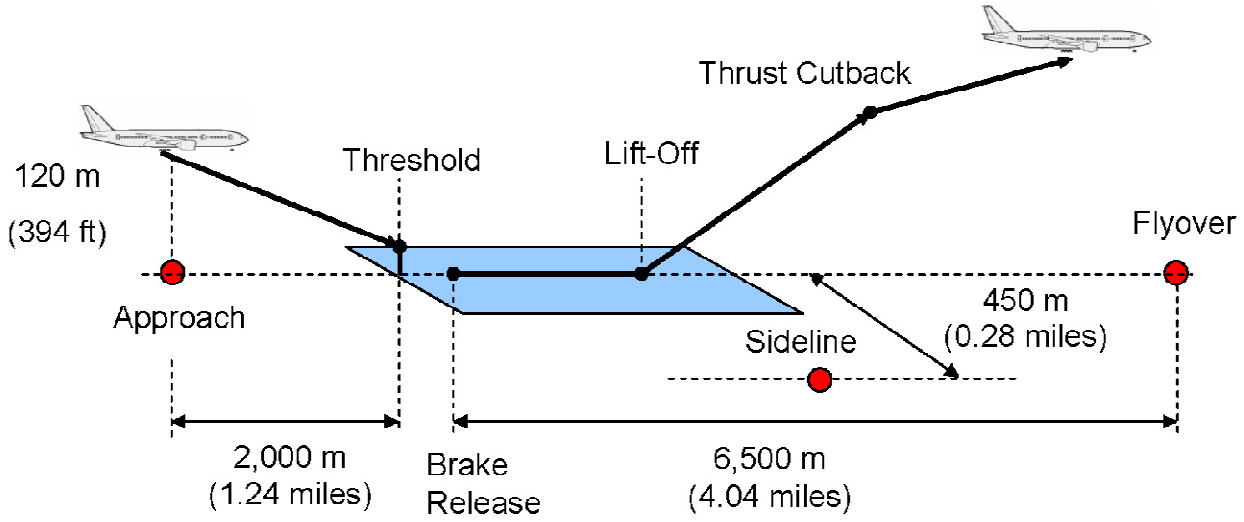

Figure 5.4: Noise Certification Points[15]

The most current requirements, Stage 4, must be 10 dB lower than the Stage 3 requirements. Figure 5.5 shows the requirements for approach noise as a function of the aircraft's weight. Similar plots exist for sideline and flyover noise.

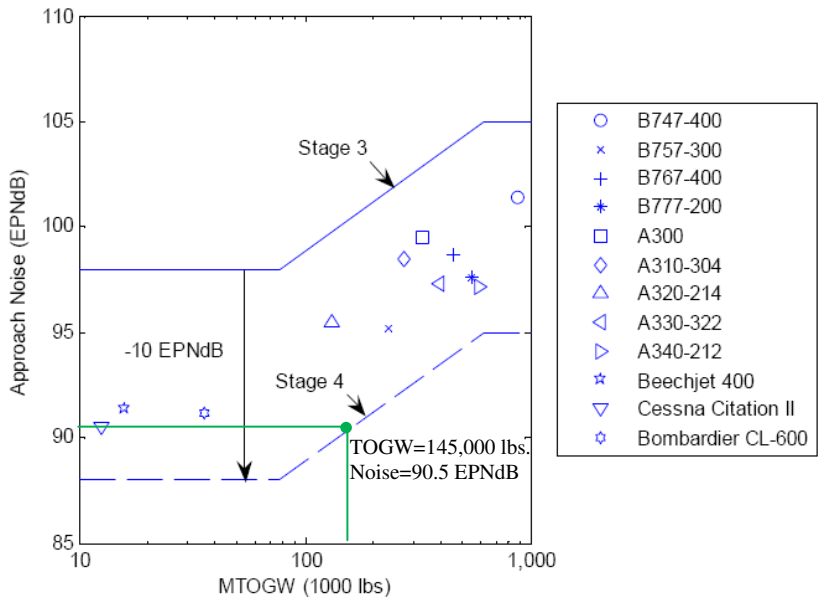

Figure 5.5: Current ICAO Noise Standards[15]

As outlined in the propulsion section, engine noise will be reduced by using the PW1000G engine. This engine will automatically reduce aircraft noise by the required 20 dB. The HB-86 is also a much cleaner surface than conventional aircraft, specifically, where the fuselage meets the wing. In a conventional aircraft the wing and fuselage intersect at almost 90 degree angles. With our design, the wing is integrated around the fuselage with little to no interference of the air flow, creating a much quieter ride for the passengers.

6. Performance

6.1 Introduction

The required mission performance characteristics of the HB-86 were defined by the RFP and included range and cruise conditions, as well as takeoff and landing requirements. As the HB-86 is of a unique, hybrid-wing design, a MATLAB based performance program was developed around the performance equations given in Raymer[5]. The specific results for the HB-86, based on the developed algorithm, are displayed in Table 6.1 below:

Table 6.1: *HB-86* Performance Results

Parameter	RFP Required	Actual
Max TOGW	N/A	148,000 lbs
Takeoff Distance (BFL)	7,000 ft	6,300 ft
Acceleration Height (1200 ft AGL)	N/A	2,700 ft
Approach Distance	N/A	1,200 ft
Approach Speed	N/A	156 kts
Touchdown Speed	135 kts	135 kts
Landing Distance	N/A	5,400 ft
Initial Cruise Alt	35,000 ft	38,000 ft
Max. Alt	43,000 ft	43,000 ft
Cruise Speed	M 0.78	M 0.78
Max Cruise Range	2,800 nm	2,900 nm

6.2 Takeoff and Landing

Despite being the two shortest segments of the mission given for the *Navigator*, these sections are imperative to ensure the aircraft may continue to operate out of existing aircraft facilities. According to the RFP requirements, the aircraft must be able to takeoff in 7000 feet at 86° F. To calculate the takeoff-roll distance, the standard takeoff distance equation given by Raymer[5] was used (given below):

$$S_G = \frac{1}{2gK_A}\ln\frac{K_T+(K_A+V_f^2)}{K_T+(K_A+V_i^2)} \tag{6.1}$$

$$K_T = \frac{T}{W} - \mu \tag{6.2}$$

$$K_A = \frac{\rho(\mu \cdot C_L - C_{D0} - KC_L^2)}{2(W/S)} \tag{6.3}$$

$$BFL = \left(\frac{0.863}{1+2.3G}\right)\left(\rho g C_{L,climb} + h_{obstacle}\right)\left(\frac{1}{\frac{T_{avail}}{W-U}} + 2.7\right) + \left(\frac{0.655}{\sqrt{\frac{\rho}{\rho_{SL}}}}\right) \tag{6.4}$$

The longest distance for a takeoff or landing roll is at Maximum Takeoff Gross Weight (MTOW), which was decided to be approximately 145,000 lbs including 33,000 lbs of fuel. Given these conditions, the HB-86 can successfully complete a takeoff roll in 3,110 ft, with a balanced field length of approximately 6,247 ft, requiring a C_L of only 0.326.

The landing phase of flight operates in three primary phases: approach, flare, and ground roll. During the approach and flare, the aircraft descends to runway height from a set obstacle clearance altitude to the runway surface at decreasing speeds along a set radius arc to control the load factors of the descent. The approach phase begins from the obstacle down to the flare height by either a set flare height or distance from the obstacle at a speed of 156 knots (*1.2*stall speed)*[5]. The flare stage lowers the aircraft the remaining distance to the ground at a speed of 148 knots at a set load factor to prevent damage on touchdown with a velocity of 135 knots.

The ground roll phase is considered in the same way as ground roll for take-off. Equations 6.1-6.3 are again used to determine the roll, except initial velocity is now V_{TD} (touchdown velocity) and final velocity is 0. To slow the plane, brakes increase the ground friction coefficient, μ, until the plane comes to rest. The total landing field length is considered in terms of the sum of all three phases together[5]. This reveals an average landing C_L of 0.358, with a total landing distance of 8,462 ft, including 5,433 ft of runway rollout at sea level with a temperature of 86° F.

6.3 Climb/Descent

Once airborne and clear of any obstacles, the HB-86 is expected to accelerate and climb to its initial cruising altitude and speed. According to the RFP, these values are expected to be at least 35,000 ft and Mach .78. Using a maximum fuel load at TOGW, the *Navigator* can reach an initial altitude of 38,000 ft. This climb takes approximately 7 minutes at maximum rate of climb with a fuel burn of 2,192 pounds of fuel. However, this results in an average climb rate of over 5,400 ft/min. As this would most likely be uncomfortable for passengers, the pilot may instead climb at approximately 2500 ft/min for 15 minutes to reach the same altitude at a fuel savings of 300 lbs of fuel[5].

A common practice in long range airliners is that of the stepped climb. This is a climb after this initial climb made to allow fuel savings, traffic or weather avoidance. After the first 1200 nm of the planned 2500 nm mission outline, the *HB-86* has the ability to climb again up to a flight level of 430 or 43,000 ft.

The descent in the HB-86 can be performed either power off or on, depending on the descent profile desired by the pilot and/or ATC. As such, the HB-86 is expected descend at 1500 ft/min over a roughly 90 mile distance. This matches current airliner descent patterns from cruise altitude with a 3 degree angle of descent.

6.4 Cruise

According to RFP requirements, the *HB-86* will be expected to travel up to 2800nm "with typical mission reserves" at a long range cruise of Mach .78. The *Navigator* meets these requirements at 38,000 ft at Mach .78, using a fuel load of 33,000 lbs of fuel. At this altitude and speed, the HB-86 performs at a C_L of 0.147 with a specific range of 0.14 nm/lbs fuel. A further requirement specified by the RFP is for a short-haul flight of only 500nm, with a fuel requirement of 41 lbs fuel per seat or less. For this flight, the *HB-86* meets that objective requiring only 7500 lbs of fuel with reserves, leading to a specific range of 0.12 nm/lbs fuel or 41 lbs/seat [5]. The chart below, Figure 6.1 shows further specific range results if the *Navigator* were to cruise at alternate altitudes and speeds. Altitudes above initial cruise of 38,000 ft assume a stepped climb partway through the cruise portion of the flight. As the chart shows, higher altitudes result in more fuel efficiency, this is due to atmospheric conditions at higher altitudes and the fuel spent climbing to those altitudes. An additional advantage of the higher altitude is that the cruise speed may increase to Mach .8 with a negligible effect on specific range.

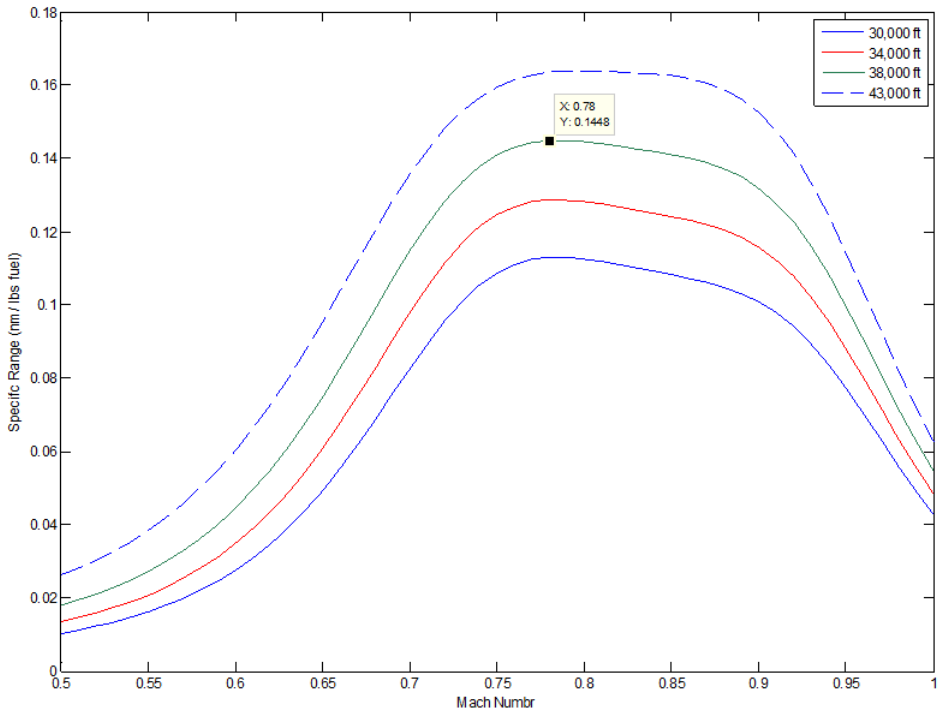

Figure 6.1: Specific Range

7. Aerodynamics

7.1 Planform Design

The design of the airframe planform was an iterative process between configuration and performance. Having determined the maximum loading on our wing (Section 3), we were able to estimate the approximate area of the wing. Historically, hybrid-wing aircraft do not have high aspect ratios. From performance analysis (Section 6), a goal aspect ratio of 3.6 was determined to meet specific RFP range requirements. Having a goal wing area and aspect ratio, this allowed simple determination of an ideal wing span. From the primary geometric wing constraints, the shape of the planform was investigated to meet structural, volume, and system integration requirements. To finalize the planform geometry, the Korn equation was used to determine constraints on thickness and wing sweep. The Korn equation, as found in Mason[16], is the following:

$$M_{DD} = \frac{K_A}{\cos\Delta} - \frac{(t/c)}{\cos^2\Delta} - \frac{C_l}{10\cos^3\Delta} \qquad (7.1)$$

Where M_{DD} is the drag-divergence Mach number, K_A is a technology factor associated with the airfoil (0.95 is the technology factor used for a supercritical airfoil), and Δ is the sweep of the wing. With a desired cruise Mach number of 0.78, we determine the two-dimensional Mach number to be equal to 0.63. With this value, and a cruise lift coefficient of 0.2043, we find that a thickness to chord ratio of approximately 0.14 and wing sweep of approximately 36° yield a drag-divergence Mach number of 0.86, well above our desired cruise velocity.

Figure 7.1 displays a top view of the planform geometry:

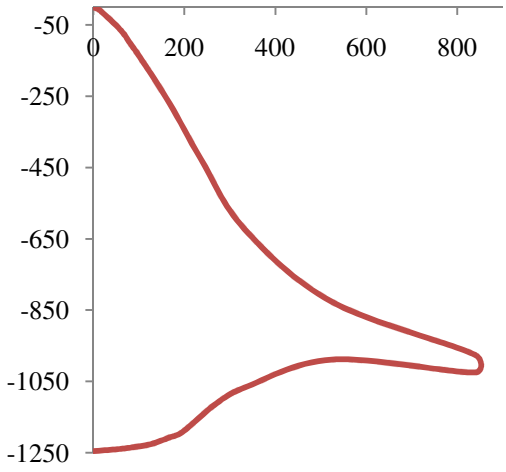

Figure 7.1: Planform Geometry (Station Locations in Inches)

7.2 Airfoil Selection

Having determined the planform geometry for the *HB-86*, it was now necessary to determine the shape of the wing by selecting the airfoil. In the first iteration of the design, the center fuselage was to serve as a lifting body; however, complications involving pressure vessel integration prevented this. Faced with a non-lifting center, the wing was now to be designed as the primary lifting surface.

Several factors influence the airfoil selection process. Operations within the transonic regime lead to the use of a supercritical airfoil to increase the critical Mach number for the airframe. Knowing the thickness constraints of the planform, we examined two classical supercritical airfoils (NASA/Langley SC (2)-0714 and the NASA/Langley Whitcomb Integral). The decision was made to overlook typical NACA airfoils based on regime operations. From the individual airfoil analyses of our selections, we determined the airfoil of choice for the wing to be the RAE(NPL)-5213 transonic airfoil[17]. During its design, RAE 5213 was given a thickness of 14.65 percent with a design Mach number of 0.776[18]; these two conditions agree with our desired cruise Mach number 0.78, and our drag divergence Mach number of 0.86. Several benefits resulted from this decision, including ample volume for fuel system integration, a lift coefficient regime comparative to our performance results, and efficient operations within the transonic regime. Figure 7.2 displays a view of the selected airfoil:

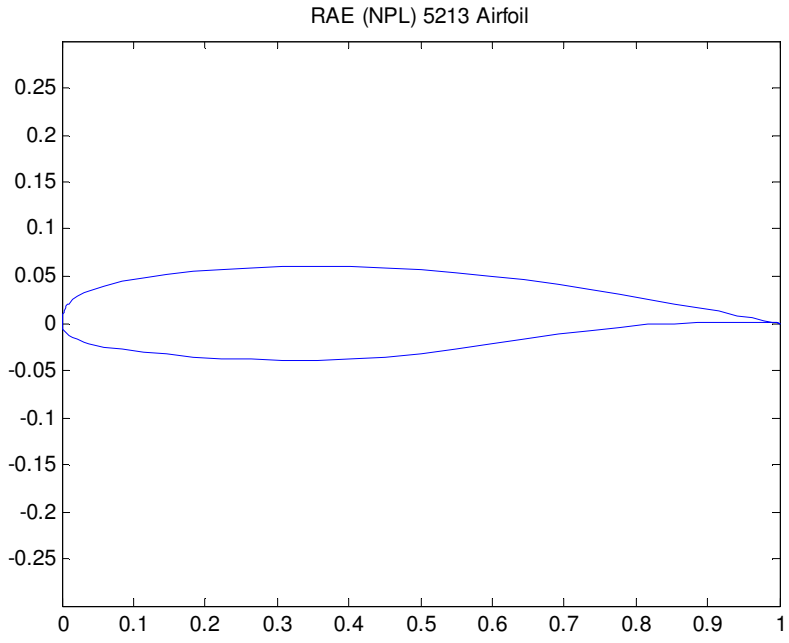

Figure 7.2: RAE(NPL) 5213 Plot

Figure 7.3 below depicts the two-dimensional lift coefficient plotted against angle-of-attack determined via TSFoil[19], a tool for transonic airfoil analysis. The data in Figure 7.4 are wind tunnel test results of the RAE-5213 that correspond to low angles of attack of the TSFoil analysis and validate the results of Figure 7.3. Figure 7.5 displays the results of the pitch-moment coefficient versus the angle of attack:

Figure 7.3: Lift Coefficient Verses Angle of Attack for RAE-5213 Airfoil

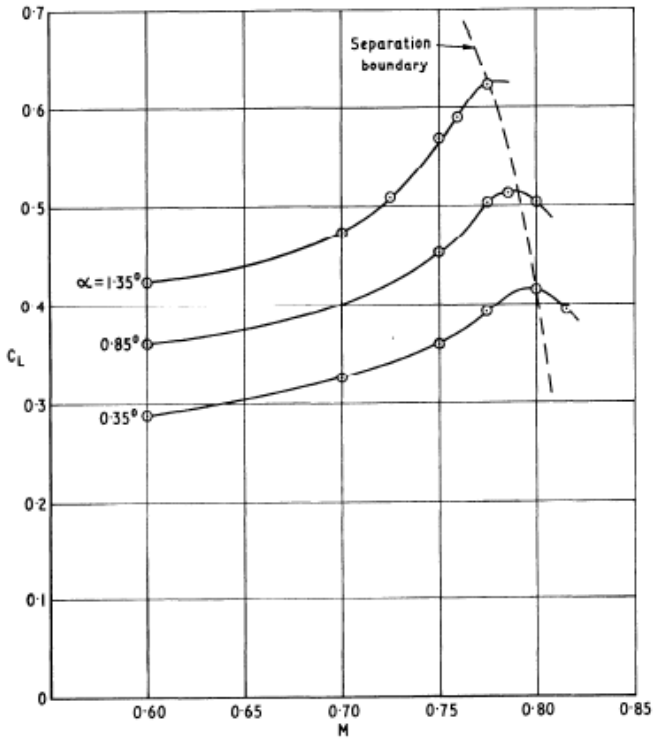

Figure 7.4: RAE 5213 Wind Tunnel Test Results[18]

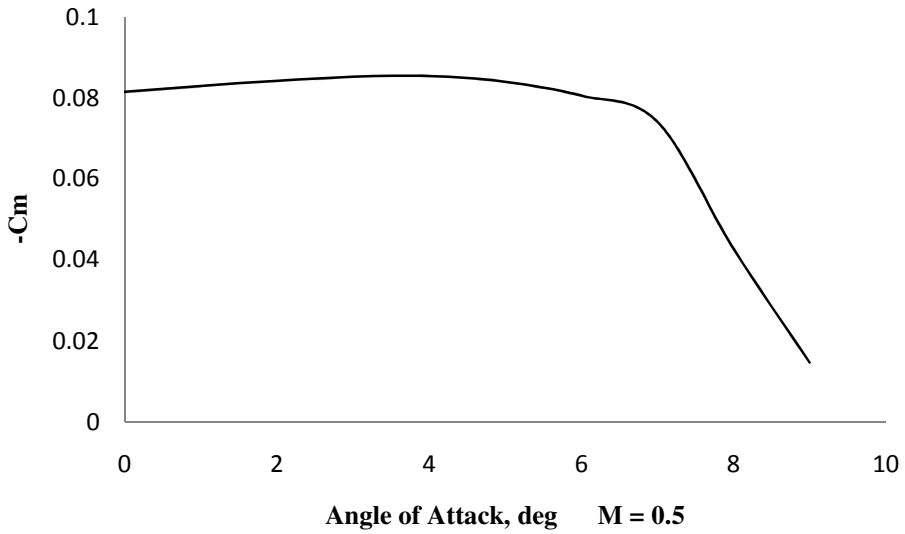

Figure 7.5: Pitch Moment Coefficient of RAE-5213 Airfoil

As well, Figure 7.6 displays the distribution of the pressure coefficient along the length of the airfoil at a nominal two-dimensional Mach number of 0.63 and zero degree angle of attack. The pressure coefficient was determined using TSFoil.

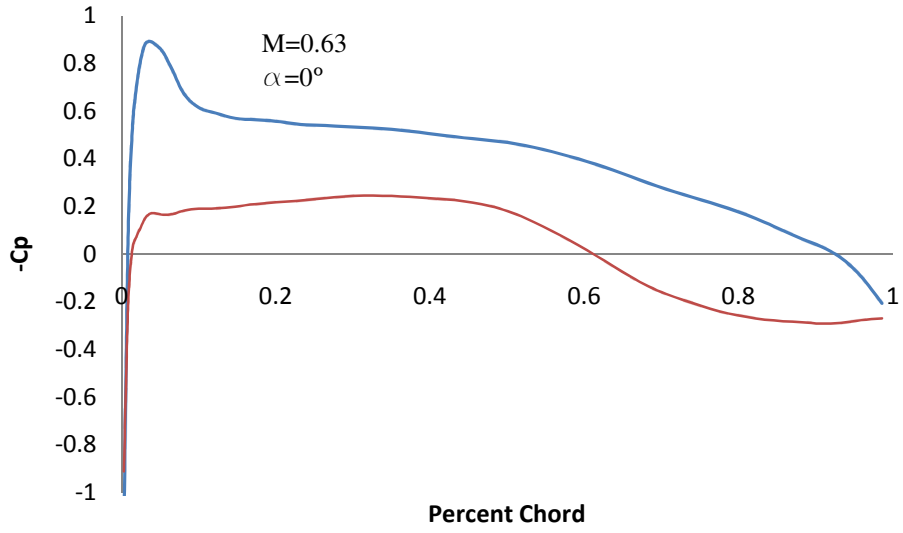

Figure 7.6 Pressure Coefficient Along Chord of RAE-5213 Airfoil (M=0.63, α=0°)

7.3 Drag Analysis

The blended nature of the design makes significant impact on the philosophy of drag build-up and analysis. With the hybrid design, we assume that the wing and fuselage volume will be treated as an individual wing-body unit. Our lack of horizontal and vertical tail control surfaces also negate typical drag build-up algorithms. The propulsion system contribution is accounted for in the nacelle component of the drag build-up. The windshield contributes to the drag build-up; however, the custom hybrid configuration produces a design that yields a parasitic drag build-up of very little and negligible magnitude. The inherent lack of flap mechanisms negates the leading and trailing edge flap drag components. For cruise, landing, and takeoff configurations, the only difference in orientation and configuration is the addition of landing gear. Thus, our main assumption in the drag build-up is the equivalency in parasitic drag between landing and takeoff. The drag build-up was determined via a combination of methods from Roskam[20] and Raymer[5], and the results were comparative with results from a skin friction analysis program (*Friction.f*[21]) Table 7.1 displays the values for the drag components, while Figures 7.7 and 7.8 yield drag polar plots for the three main portions of the mission. The components considered in the drag build-up are the wing-body, nacelle, and landing gear. The wing-body has been broken down into three sections along the wingspan to provide greater detail:

Table 7.1: Parasitic Drag Component Breakdown

Station	Takeoff/Landing	Cruise
Wing-Body (tip-chord to span of 40 feet)	0.00261	0.00138
Wing-Body (wingspan of 40 feet to 20 feet)	0.00357	0.00280
Wing-Body (wingspan of 20 feet to root-chord)	0.00478	0.00319
Nacelle	0.00107	0.00269
Landing Gear	0.01400	0.0000
Total C_{D0}	**0.02603**	**0.01006**

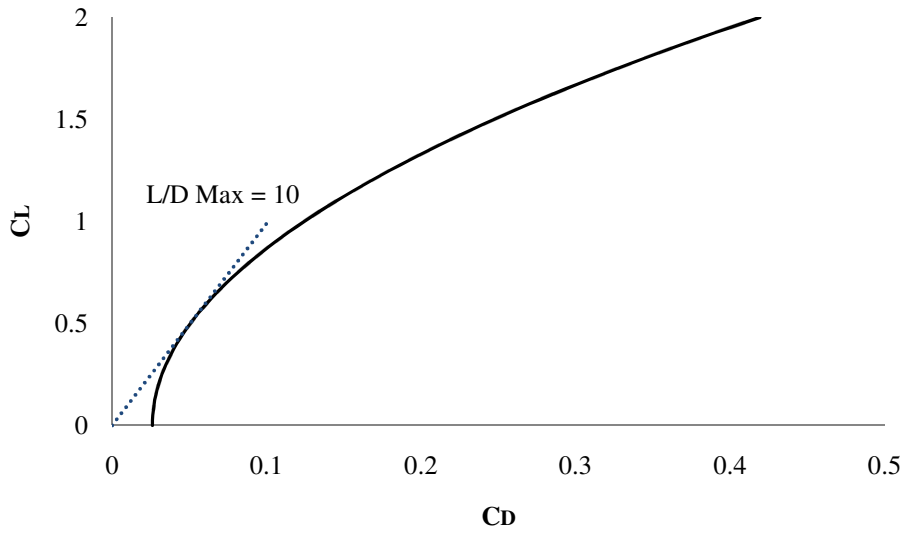

Figure 7.7: Drag Polar for Takeoff, Landing (M = 0.5, h = sea level)

Now, consider the drag polar plot for cruise conditions, and note the similarities:

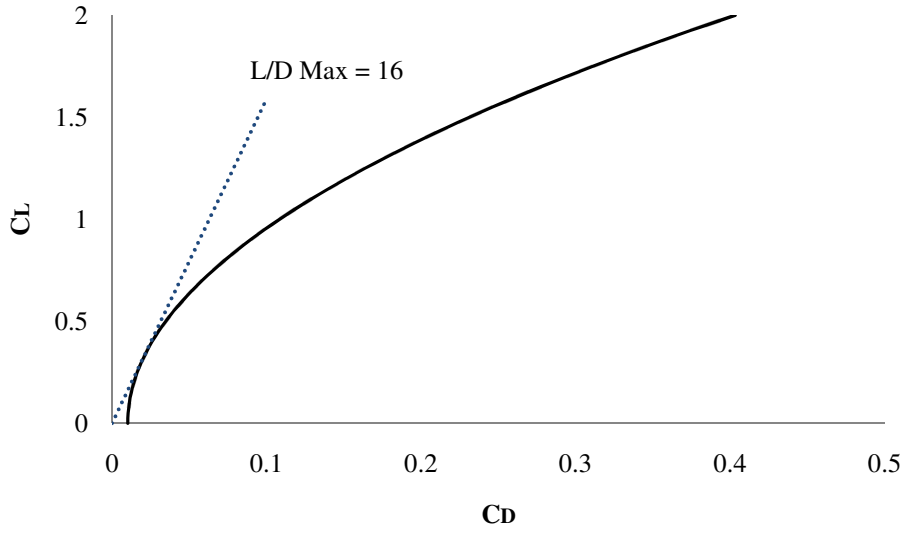

Figure 7.6: Drag Polar for Cruise Condition (M = 0.78, h = 38,000 ft)

The drag polars were calculated using the standard equation below:

$$C_D = C_{D,0} + \frac{C_L^2}{\pi \cdot AR \cdot e} \qquad (7.2)^5$$

Where *e* is the Oswald efficiency factor (Calculated to be approximately 0.9). From Figures 7.7 and 7.8, the maximum lift to drag ratio is found to be 10 during takeoff and landing, and 16 during cruise conditions. Historically, hybrid wing aircraft are known to have a maximum lift to drag ratio of greater than 20. The magnitude difference between the *Navigator* and other hybrid wing aircraft is the nature of the design; our design is intended for a much lower passenger number, greatly increasing our aspect ratio to maintain the same aerodynamic benefits of higher scale hybrid aircraft. From Equation 7.2, it can be noted that a lower aspect ratio will result in a higher value for drag. The higher the drag value, the lower the ratio between lift and drag. Considering the results of the drag build-up and polar plots of lift coefficient to drag coefficient, it can be noted that the HB-86 has, undoubtedly, a minimal parasitic drag coefficient. So that while velocity (and lift coefficient) will increase during flight, the value for the parasitic drag of the *Navigator* will remain relatively low, and enable us to reach greater ranges, longer endurance, and higher fuel efficiency.

8. Stability and Control

8.1 General Issues

Hybrid-wing aircraft are subject to many unique stability problems due to their design. These issues rise from the locations of both the aerodynamic center and the center of gravity. In many designs for hybrid wing aircraft, the wing has a high thickness to chord ratio and low sweep to take maximum advantage of the increased wing area. This moves the aerodynamic center ahead of the center of gravity, and the aircraft becomes statically unstable in flight as revealed by a negative static margin. Also, the hybrid wing design typically does not use a vertical stabilizer for yaw moment controls. Instead, disturbances are controlled through split rudders attached to the aircraft's winglets[22].

8.2 HB-86 S&C Features

The *HB-86* features outboard and inboard elevons, which can control both pitch and rolling movements of the aircraft. . Using the structural needs of the aircraft as a baseline, the program *JKayVLM*[23] was used to size the control surfaces for the *Navigator.* From this, measuring the half span of the wing from the inner blend portion of the fuselage to the wing tip, the outboard elevons are located between 50-85 percent of the wing half-span and primarily used for roll moment control using 10 percent of the wing chord length at this location. Similarly, the inboard elevons are located between 10-35 percent of the half span, and are used for pitch controls occupying 20 percent of the chord at that location. However, the cross control availability helps maximize control efficiency. The vertical winglets of the

Navigator are equipped with clam-shell style air-brakes which provide differential yaw control over the aircraft. The wings themselves have a 36 degree sweep. Using values found during aerodynamic analysis, this places the aerodynamic center 63 ft from the nose of the aircraft or at 39 percent MAC. Given a 14.9 percent CG range that is forward of the aerodynamic center, the static margin[5] can be found to be between 7 and 14 percent while in flight.

The combined control surfaces on the aircraft lead to an efficient control system in all stages of flight. In order to determine the effectiveness of the control surfaces of the *Navigator*, the program JKayVLM was used to find the moment and stability coefficients of the aircraft. These values, shown below in Table 8.1, were then used in the Microsoft Excel program *VPI-NASA-CPC*[24] by Marty Waszak from NASA Langley to find the control effectiveness.

Table 8.1: JKayVLM Results

Constant	Cruise	Takeoff	Landing
Mach #	.78	.23	.24
Altitude	38,000	0	0
$C_{L\alpha}$	3.59	4.36	4.37
$C_{M\alpha}$	0.005	0.029	0.02875
C_m/C_L	0.002	0.00674	0.00657
$C_{L\text{-}q}$	1.74	1.89	1.89
$C_{M\text{-}q}$	-0.28	- 0.24314	- 0.24378
$C_{L\text{-}delta}$ (Inboard Elevon)	0.99	1.14	1.14
$C_{L\text{-}delta}$ (Outboard Elevon)	0.52	0.46	0.46
$C_{M\text{-}delta}$ (Inboard Elevon)	- 0.122	- 0.104	- 0.104
$C_{M\text{-}delta}$ (Outboard Elevon)	- 0.081	- 0.065	- 0.065
$C_{y\text{-}beta}$	- 0.02	- 0.02	- 0.02
$C_{n\text{-}beta}$	- 0.01	- 0.01	- 0.01
$C_{l\text{-}beta}$	~0	~0	~0
$C_{y\text{-}r}$	0.01	0.01	0.01
$C_{n\text{-}r}$	-0.009	- 0.00898	- 0.00898
$C_{l\text{-}r}$	0.0004	0.0004	0.00043
$C_{l\text{-}p}$	-1.03	- 0.98	- 0.97
$C_{n\text{-}p}$	-0.73	- 0.71	- 0.71

For takeoff, the elevator is deflected 34° up to create a pitching moment resulting in 5.7 degrees per second for rotation to a takeoff angle of attack of 10°. In order to maintain the required $C_{L\text{-}Trimmed}$ of .147, the *Navigator* must maintain approximately a 0 degree angle of attack. The *HB-86* fulfills this with a trim angle of -4° at cruise altitude. Once approach glide slopes are established, the aircraft needs a maintained 10 degree elevon deflection angle for an approach angle of -3°, while the flare requires an upward deflection of 20 degrees to hold initial flare conditions at an

angle of attack of 8° on touchdown. This allows for the aircraft to touch down on the main wheels first, and then gently bring the nose wheel down with further upward deflection as airspeed slows.

Since the *Navigator* is a stable aircraft, is may be assumed safe flight is possible without the use of a computerized flight control system. However, analysis using *JKayVLM* has revealed that the installation of a flight control system will be required for certain modes of flight. The need for this system is due to the damping features of the aircraft shape in all directions. While pitching disturbances will most likely be removed within a few oscillations, yawing movments of the aircraft are hardly damped at all due to the lack of a large vertical tail. While these oscillations do not affect the flight characteristics of the aircraft due to small amplitudes granted by the high sweep of the wings, the movements are, most likely, beyond human ability to completely remove. Furthermore, the coupling of the yaw and roll axis makes even further oscillations probable. As a result, a flight control system will be required, especially for the removal of yawing moments by the wingtip speed brakes.

The aircraft will also need a flight control system to help prevent adverse roll rates and oscillations in pitch when the aircraft is moved into a nose down position, due to increased camber from the deflected control surface, through the use of devices such as an alpha limiter and control input translation system similar to those in use by both the B-2 and A320[22]. This system will both help prevent the pilot from inadvertently stalling the aircraft, and aid in creating the desired aircraft change in direction despite the alteration in chamber. For example, a nose down pitching moment request from the pilot will cause the aircraft to still be able to descend while pitching down through the combined movements of several control surfaces rather than allowing the incidental "ballooning" effect the increased camber may cause. To prevent stall or other departure from safe flight conditions, the alpha limiter will prevent the aircraft from going beyond a positive 15° angle of attack and negative 10° angle of attack. This, in addition to preventing possible stall, also helps prevent the aircraft from entering unsafe nose-down attitudes from sudden disturbances.

While these systems in the *Navigator* will be required in the final design, it is worth noting that the systems are primarily for passenger comfort and to ease difficulty in flying the aircraft. If the system were to fail for any reason, the pilot would still be able to control the aircraft without much difficulty. The qualitative effect would be an increase in the number of oscillations produced and increased turbulence effect due to slower human-damping.

9. Structures

9.1 V-n Diagram

Before any structural members are designed and tested for our aircraft, various loads need to be determined. For this purpose, a V-n diagram was constructed to show the aircraft limit load factor as a function of airspeed. The V-n diagram in Figure 9.1 was constructed in accordance with Federal Acquisition Regulation (*FAR-25*) which states that a transport aircraft must have a limit load factors (n_{lim}) of positive 2.5 and negative 1.0.

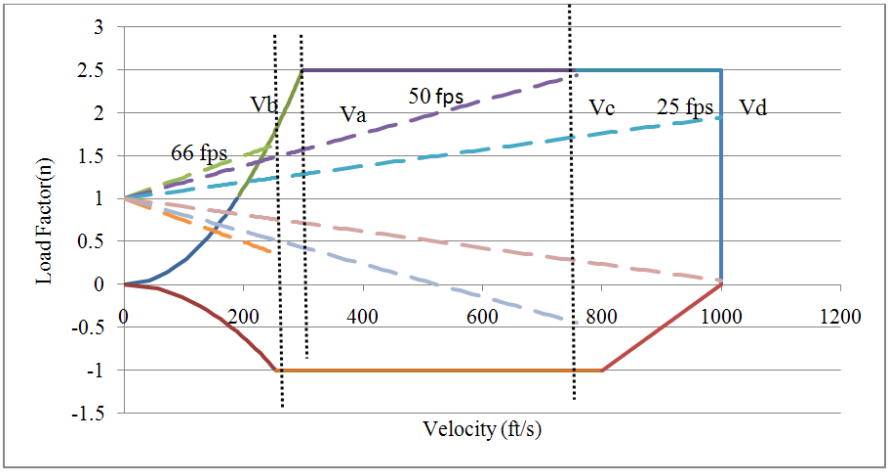

Figure 9.1. V-n Diagram

As we can see in Figure 9.1, the V-n envelope is constructed for three different gusts at 66 ft/sec, 50 ft/sec, and, 25 ft/sec. Limit load factors during the gusts are all inside the maneuver envelope so there is no need to raise the load factors above positive 2.5 and negative 1.0 for the *Navigator*.

9.2 Structural Layout

The structural layout of the *HB-86 Navigator* can be seen in Figure 9.2. The drawing shows how the loads are transferred to the principle load carriers. The principle load carriers are wing spars, wing ribs, wing skin, fuselage frames and longerons. The loads from the air are first exerted on the wing skins and then transferred to the spars through the wing ribs. The loads are then transferred to the fuselage through the frames and longerons. The fuselage is a semimonocoque structure through which loads are carried by fuselage skins, frames and longerons. The fuselage skins are reinforced with longerons, pressure bulkheads and frames. The wing structure consists of two I-beam spars as well

as the ribs. The front spar is located at 15 percent of the chord and the aft spar is located at 65 percent of the chord. Wing ribs are aligned parallel to the flight path to provide better aerodynamic flow over the body and are spaced 24 inches[25]. The wing spars are connected to the fuselage at the frames.

The structure of the fuselage consists of frames and longerons. The frames are spaced 25 inches and the longerons are spaced 12 inches. Because of the weight saving benefits longeron-frame structure is preferred instead of stringer-frame structure for *HB-86Navigator*[25]. The pressure cabin for the *Navigator* is decided to be pressurized to 8000 ft internal pressure. The thickness of the pressure cabin wall is 0.339 inches. The pressure cabin wall is internally supported by vertical beams at the intersection of the circular cabins in various locations for structural strength as seen in Figure 9.3. Due to the shape of the airframe, three different pressure cabins had to be designed as can be seen in Figure 9.4 below. This required us to have four pressure bulkheads for our design. The detail location of the pressure bulkheads can be seen in Table 9.1 below. The primary load carriers- the wing skin and fuselage skin are each 0.25 inches thick.

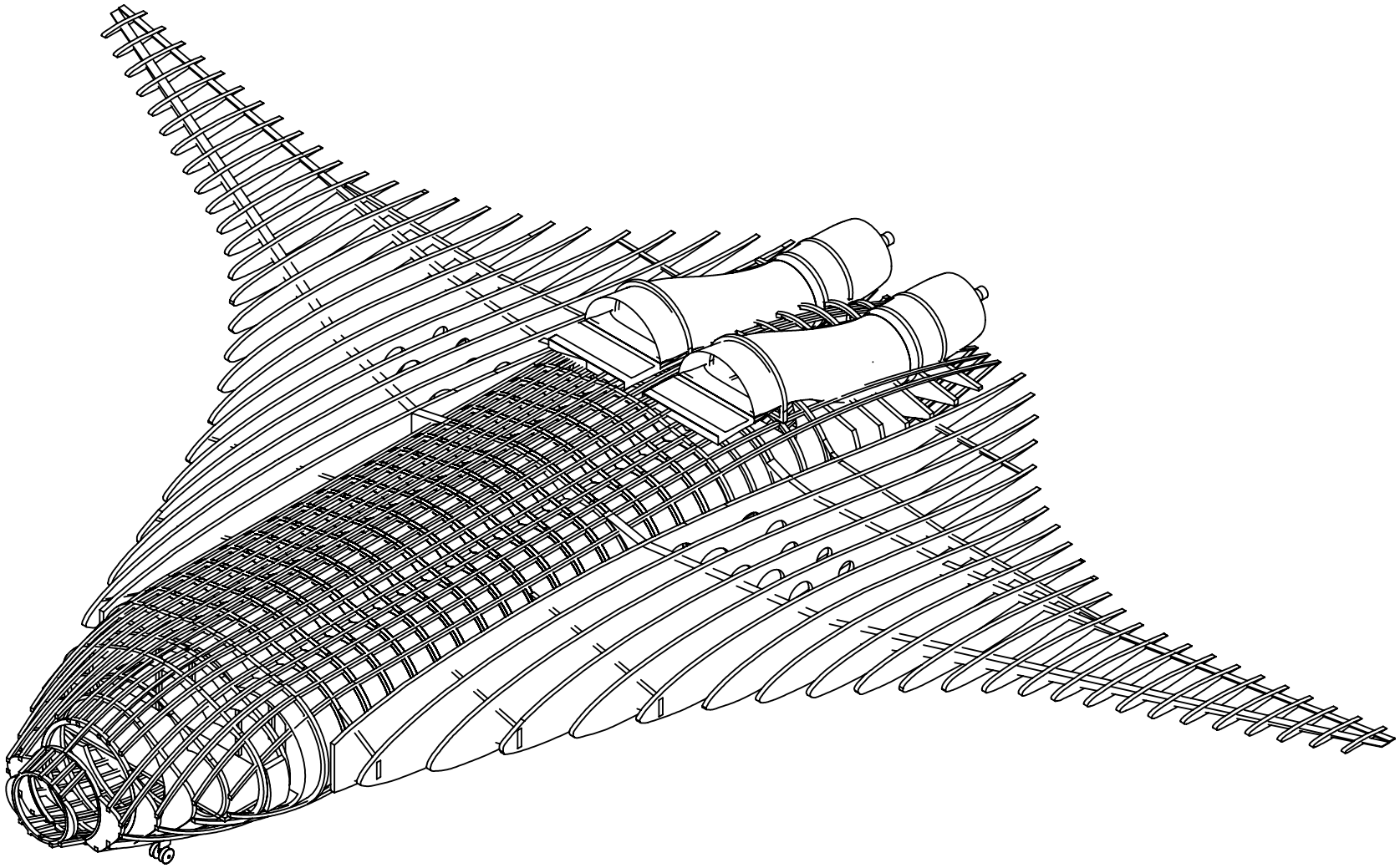

Figure 9.2: Navigator Structural Layout

--

--

	NAME	DATE	Fusion Aeronautics		
DRAWN	S. Kafle	3-28-09	SIZE A	DWG. NO.	REV.
CHECKED	L. Thomas	3-29-09			
			SCALE 1:150		SHEET 1 OF 1

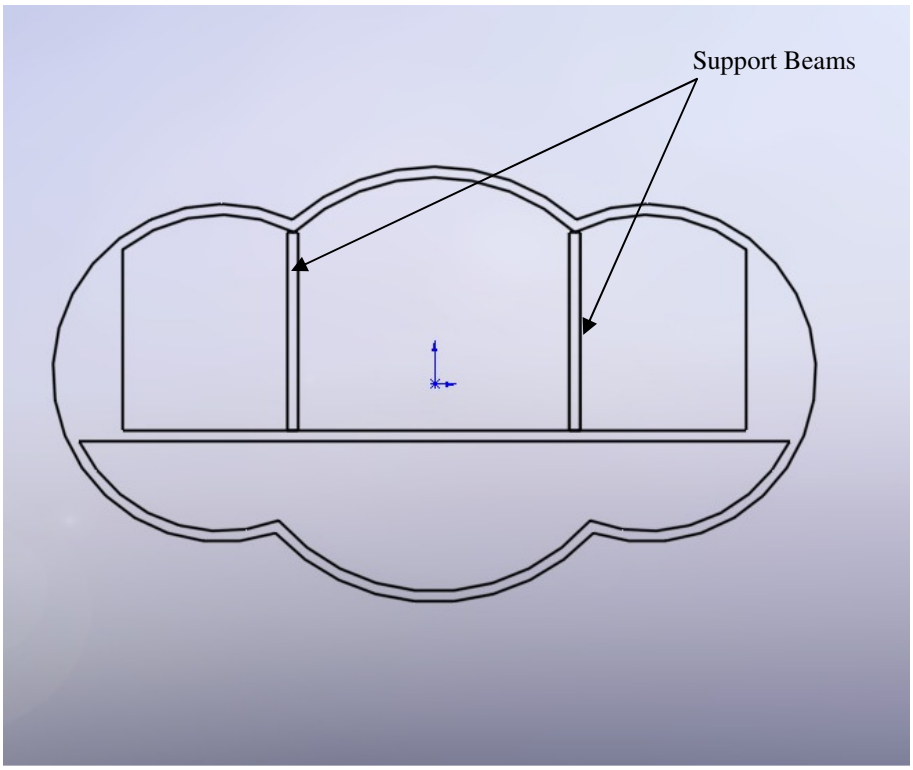

Figure 9.3: Pressure Cabin Walls with Support Beams

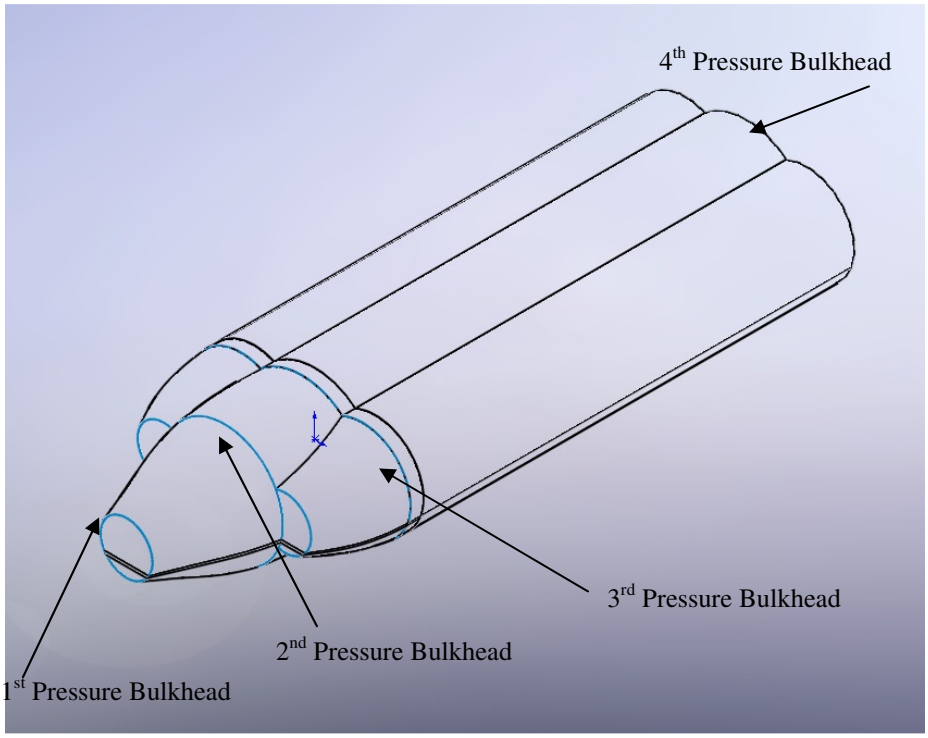

Figure 9.4: Pressure Cabin Layout and Pressure Bulkheads Placement

Table 9.1: Location of Pressure Bulkheads

Pressure Bulkhead	Location from the nose tip
First	5.35 ft
Second	16.03 ft
Third	24.43 ft
Forth	75.08 ft

9.3 Choice of Materials

Aircraft TOGW is directly dependent on the selection of materials. With advancement in technology, composites are widely used for aircraft. Use of composites has great benefits to the weight of the aircraft. Materials used in the *Navigator* were chosen from research on current Airbus aircraft [26].

Most of the materials chosen for the aircraft are carbon fiber reinforced polyethylene (CFRP). CFRP has a weight reduction of 10-20 percent compared to traditional Al alloys which leads to cost savings of $28-$46 per pounds[27]. With CFRP, adhesives are used extensively instead of nuts and bolts (as in Al alloys) which aid in reducing the structural weight of the *Navigator*. CFRP also has advantages for the performance of an aircraft. CFRP offers improved fire containment and higher crash safety for the structural members. In the *Navigator* CFRP is used in pressure bulkheads, upper deck floor beams, outer flaps, elevons, wing spar, wing ribs, lower wing skins, longerons, engine cowlings, and fuselage frames as we can see in the Figure 9.5.

Another structural material found in the *Navigator* is a hybrid metal and fiber glass laminate called GLARE. It offers high fatigue resistance compared with Al alloys, has greater damage tolerance[27,28] and also has high resistance to corrosion and fire. The structures in the *Navigator* composed of *GLARE* are fuselage skins, wing skins, and doors. Thermoplastics are also employed in the structural foundation of the *HB-86 Navigator.* Thermoplastics have high strain to failure and high fracture energy[25]. The thermoplastics also absorb less moisture and have high resistance to delaminating. On the *Navigator* thermoplastics are used as the materials for wing leading edges as seen in Figure 9.6.

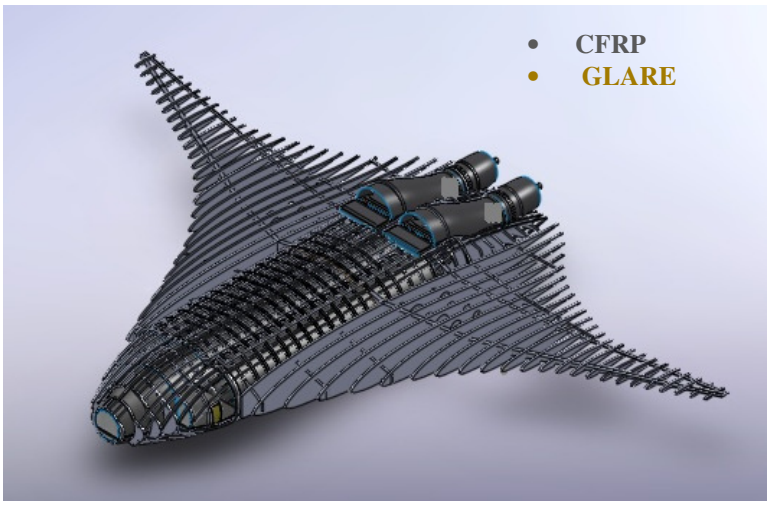

Figure 9.5: Internal Structures Materials for *HB-86 Navigator*

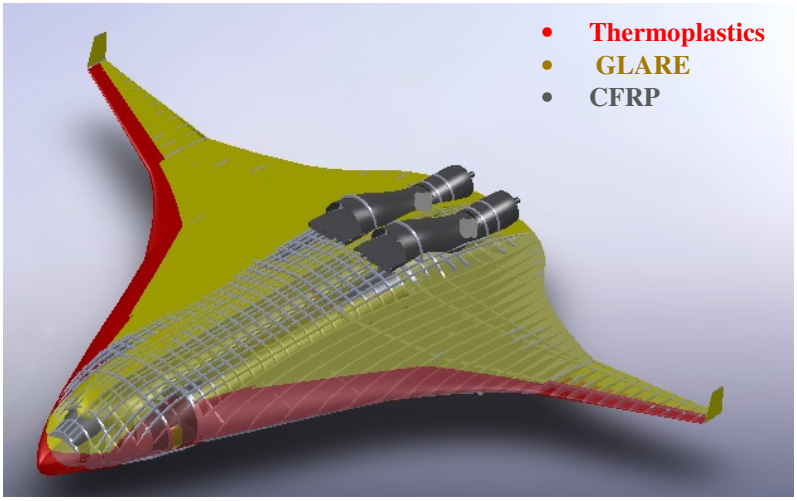

Figure 9.6: Wing and Fuselage Skins Materials for *HB-86 Navigator*

9.4 Stress Analysis

Preliminary stress analysis was done on the principal load carriers for the *Navigator*. The loading on the surface of the *Navigator* is assumed to be elliptic as seen in Figure 9.7 below. The maximum shear load is acting at the root chord location and is decreasing toward the wing tip as seen in Figure 9.8. The maximum bending moment occurs at the joint where the spar is attached with the fuselage frame. The bending moment curve can be seen in Figure 9.9 below. Principle load carriers for the *Navigator* are wing/fuselage skins, wing spar, longerons, and the pressure cabin wall. Stress analysis for the skin was performed assuming the skins are installed in the aircraft as panels. Each panel is 119.29 inches long, 47.29 inches wide and 0.25 inches thick. The critical load needed to buckle the skin panel was

calculated and was compared with the calculated load applied as seen in Table 9.2 below. Iterations were then performed to determine the appropriate skin thickness:

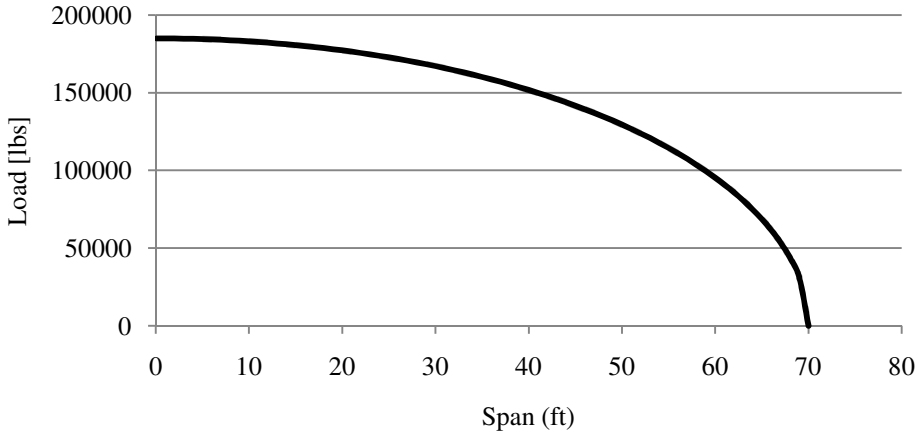

Figure 9.7: Elliptic Spanwise Loading

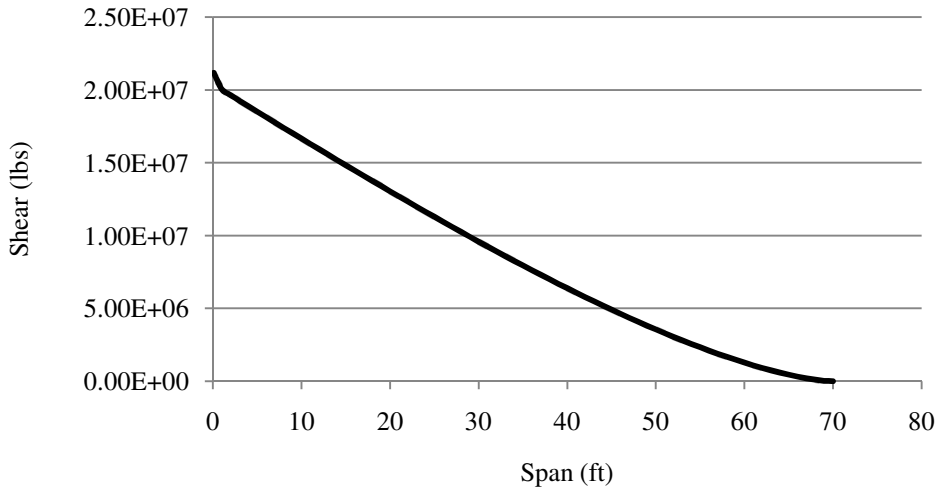

Figure 9.8: Spanwise Shear Distribution

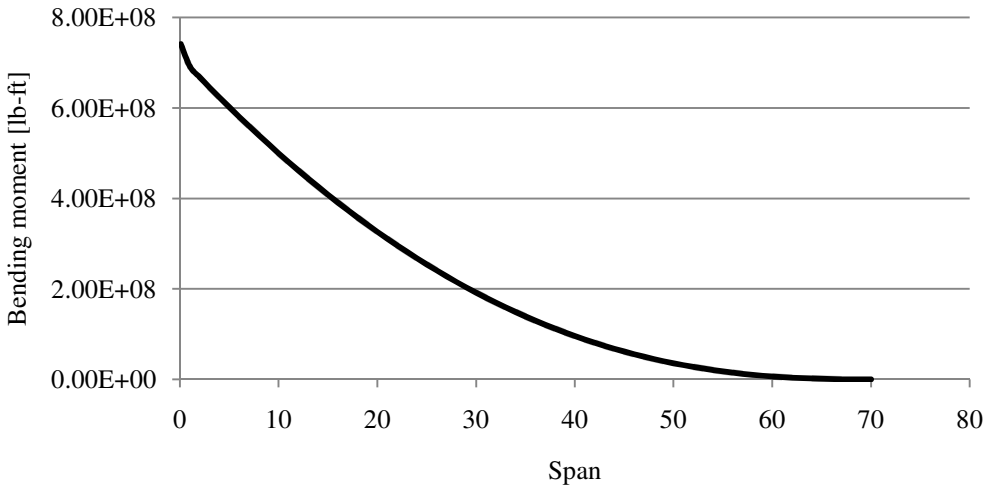

Figure 9.9: Spanwise Bending Moment

Table 9.2: Stress Analysis for Wing/Fuselage Skin Panel

Wing Skin panels	
Materials Used	GLARE
Panel Thickness (inches)	0.25
Panel width (inches)	47.64
Panel length (inches)	119.29
Elastic Modulus (psi)	7.696
length/width	2.5
buckling coefficient	6.3
Buckling Stress (psi)	1.33E+03
Material Tensile Stress(psi)	7.98E+04
Critical Load needed to buckle the plate (lb)	**7.58E+06**
Load applied (lb)	**1.85E+05**

The I-beam spars chosen for the design are W36X300. Stress analysis was done on both the front and rear spar. Maximum applied bending stresses for the spars were calculated and were compared with the yield strength of the spar as seen in Table 9.3 below. The maximum bending stress occurs at end of the spar close to root chord so spars have highest depth near the root chord and decreases sharply as moved toward the wing tip.

Table 9.3: Stress Analysis for Wing Spar

Wing Spar(W36X300) all **Dimensions in inches**	Front Spar	Rear Spar
Flange thickness(tf)	1.68	1.5
Flange width(bf)	16.65	10
depth (d)	36.74	25
thickness of web(tw)	0.945	0.7
Section Modulus (in^3)	3.40E+06	4.38E+05
Moment of Inertia (in^4)	6.25E+07	5.48E+06
Materials used	CFRP	CFRP
Yield strength (psi)	**1.45E+05**	**1.45E+05**
Critical buckling shear stress for shear web (psi)	1.54E+05	1.82E+05
Max Applied Bending Stress (psi)	**2.61E+03**	**2.03E+04**

Stress analysis was also done for the pressure cabin wall. The aircraft was pressurized to 8000 ft and the required wall thickness which is able to carry the load was calculated. The pressure exerted on the wall was compared with the crippling stress as seen in Table 9.4. The crippling stress value for the wall was calculated using the diameter of the fuselage, thickness of the wall and the elastic modulus of the material used. The iterations were done to make sure the wall thickness was able to withstand the pressure exerted without exceeding the crippling stress value.

Table 9.4: Stress Analysis for Pressure Cabin Walls

Materials Used	GLARE
Thickness (inches)	0.339
Radius (inches)	144
Elastic Modulus (psi)	7.69E+06
Yield Stress (psi)	1.81E+04
Crippling stress (F_c) (psi)	**5.43E+03**
Applied internal design pressure (psi)	**10.91**

The fuselage of the *Navigator* has longerons all around it attached to the frames. The stress analysis was done for the longerons as seen in Table 9.5. The longerons are clamped with the frames so analysis was done for a longeron between two frames and were assumed that same analysis applies throughout. The maximum applied stress in the longeron was calculated and was compared with the maximum buckling stress value. Iterations were made by changing

the thickness of the longeron to make sure that it is able to stand the applied stress without exceeding the maximum buckling stress.

Table 9.5: Stress Analysis for Longeron

Longerons	
Materials Used	CFRP
Longeron length (inches) (clamped with frames on both sides)	25
Effective Length (inches)	17.75
width (inches)	4.08
thickness (inches)	4.08
Moment of inertia (in^4)	2.31E+01
Elastic Modulus (psi)	2.18E+05
Critical Load (Pc) (lb)	1.57E+05
Max Buckling Stress (psi)	9.45E+03
Yield Stress (psi)	1.45E+03
External Loads on Fuselage (lb)	4.04E+04

9.5 Finite Element Analysis

Finite element analysis was done for wing spar and wing skin using COSMOSXpress. Wing spars and wing skins in the *Navigator* are composed of CFRP and GLARE, respectively. This analysis does not have either of the materials available for the analysis; therefore, the analysis was done using aluminum alloy 2024. This alloy has less yield strength compared to CFRP and GLARE (Table 9.6). This indicates that CFRP and GLARE are automatically successful, if the analysis is successful with 2024. The stress distribution on the wing was done using the Von Misses method. The lift load was applied on the wing assuming 70 percent of the total lifting load is carried by the front spar and the remaining 30% of the load is carried by the rear spar, which is restrained at the wing chord. The maximum displacement or the bending of the wing spar as seen in the Figure 9.10 is 22.10 inches at the wing tip.

Analysis was also performed on the wing skin panel with a maximum load of 633.56 lbs applied per panel. The wing skin was restrained at all four sides against wing spars and wing ribs. The maximum displacement on the wing skin panel was 0.001391 inches as seen in Figure 9.11.

Table 9.6: Material Yield Strength

Materials	**Yield Strength (psi)**
Aluminum alloy 2024	$1.10E^{+04}$
CFRP	$1.45E^{+05}$
GLARE	$1.81E^{+04}$

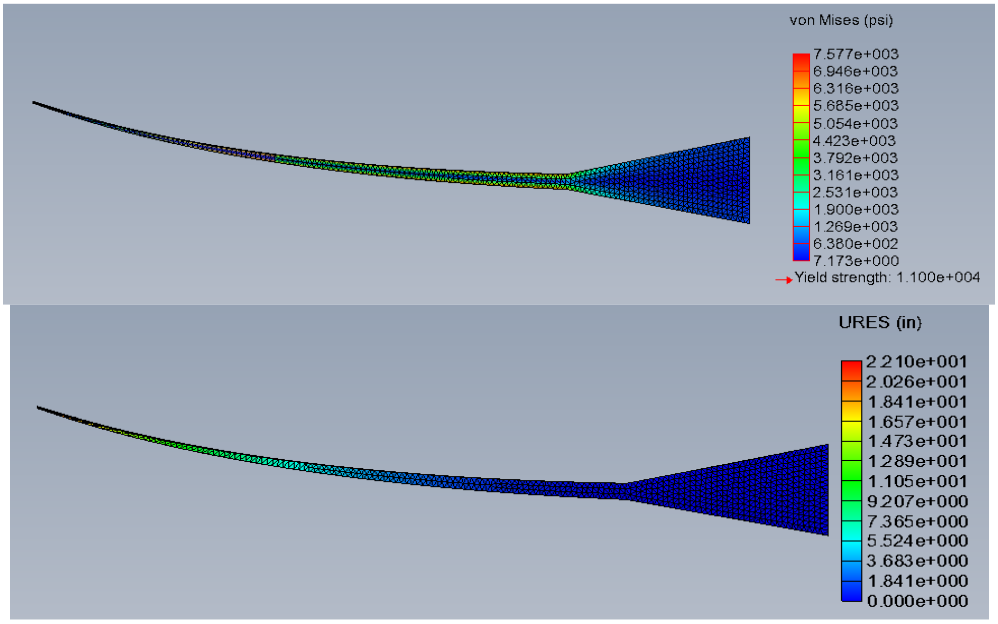

Figure 9.10: Von Misses and URES Displacement Analysis for Wing Front Spar.

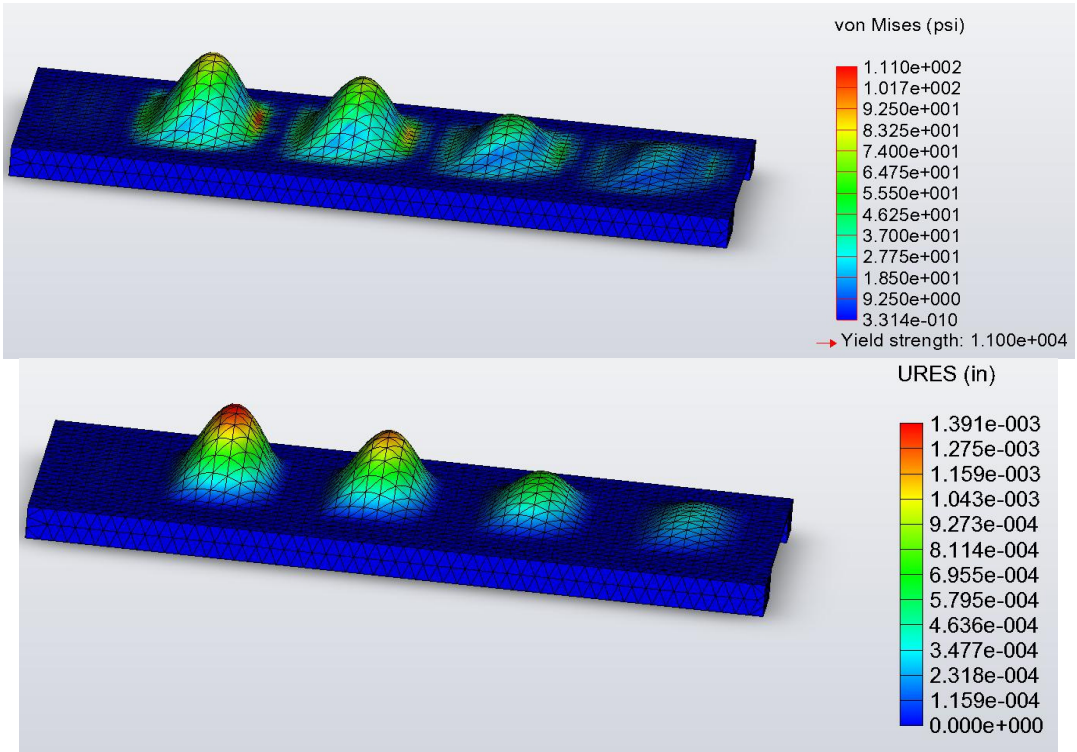

Figure 9.11: Von Misses and URES Displacement Analysis for Wing Skin Panel.

10. Systems

10.1 Landing Gear

A twin tricycle landing gear configuration was chosen to ensure efficient cargo operations, passenger boarding, pilot line-of-sight, and nose-up landing. The *HB-86* will be operating on Type III runways, requiring tire pressures between 120-200 psi. After performing a static load analysis, the reaction forces for the main and nose landing gear were determined. Allowing for 25 percent growth in airplane weight, the loads were recalculated and shown in Table 10.1:

Table 10.1: Landing Gear Load Analysis

	Nose Gear	Main Gear
Max static load (per tire), lbs	16,904	33,713
25% airplane growth, lbs	21,130	42,141

Based on this information, Type VII tires will be used on the *HB-86*. Table 10.2 shows some of the tires that were considered during the selection process from Goodyear's Flight Leader Series[29].

Nose Gear – Type VII Tire					
Tire Size (in)	Ply Rating	Rate Speed (mph)	Rated Load (lbs)	Rated Inflation (psi)	Weight (lbs)
34 x 11	22	225	20,500	185	81.4
36 x 11	22	190	23,300	200	89.6
36 x 11	**22**	**225**	**23,300**	**200**	**87.5**
36 x 11	24	201	26,500	235	72.9
Main Gear – Type VII Tire					
Tire Size (in)	Ply Rating	Rate Speed (mph)	Rated Load (lbs)	Rated Inflation (psi)	Weight (lbs)
46 x 16	28	195k	41,800	210	154.4
46 x 16	28	225	41,800	210	198.4
46 x 16	**30**	**225**	**44,800**	**225**	**207.7**
46 x 16	32	225	48,800	245	208.0

Table 10.2: HB-86 Selected Tire Data (Design Point Bolded)

From the above data the best choice for the nose gear was 36"x11" wheels, and 46"x16" wheels for the main landing gear.

Accompanying this landing gear selection, an electrical braking system by Messier-Bugatti[30] was chosen. With an electric braking system, hydraulic lines and equipment are replaced by electronic control units and electrical wiring. Electromechanical actuators replace the hydraulic pistons. On braking, a control system converts the electrical signals to an electromechanical command. Figure 10.1 shows the principle behind the electric brakes. For Figure 10.1, (1) indicates the location of the electric motor, (2) the location of reduction gear, (3) a ball screw and nut, and (4) and (5)

are rotor and Stator carbon disks. The electric brake system weighs less, has increased control, and higher reliability than conventional brake systems.

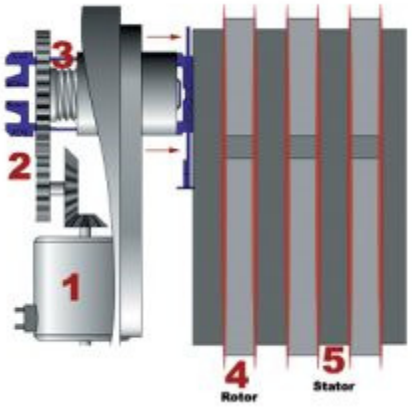

Figure 10.1: Electrical Brakes[30]

10.2 Fuel System

Using the weight fraction method, 34,200 pounds of fuel (5,040 gallons) was required as per the RFP mission profile. This resulted in 680 cubic feet of physical volume required to hold the fuel. The fuel is to be distributed evenly across the fuel tanks in both wings, ensuring little CG shift. Figure 10.2 shows the placement of the fuel tanks.

A nitrogen generating system by Hamilton Sundstrand[31] will render the fuel tanks inert. This system safeguards against the possibility of an unintentional ignition of fumes remaining in a partially empty fuel tank. The system works by pumping air through a molecular sieve designed to concentrate the nitrogen. The collected nitrogen is then pumped into the tanks as the fuel is gradually used up over the course of a flight.

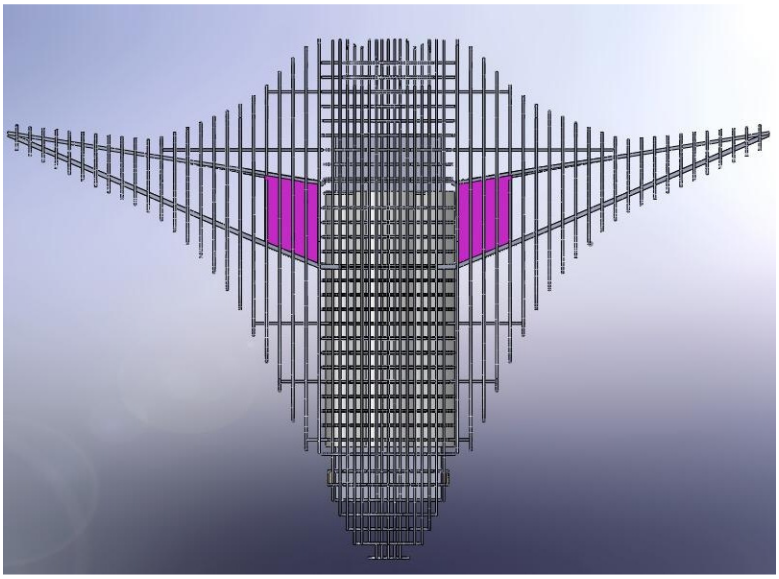

Figure 10.2 – Fuel Location

10.3 Electrical System

Up until recently, traditional aircrafts rely on bleed air systems. Due to technological advancements, newer aircraft can incorporate a no-bleed system[32], eliminating pneumatic systems and bleed manifolds, and converting the power source of most functions formerly powered by bleed air to electrical power. Some of the benefits of this system include:

- An improved fuel consumption due to a more efficient power extraction
- Reduced maintenance costs due to the lack of the maintenance-intensive bleed system
- Improved reliability due to the power electronics along with fewer components in the engine installation
- Reduced maintenance costs and improved reliability due to fewer parts used
- Thrust can be produced more efficiently
- Weight savings

Boeing expects the no-bleed system to extract about 35 percent less power from the engines as well as a predicted fuel savings of about 3 percent.

Systems such as the APU, electrical power generator, primary power distribution, and electric starter generators are also from Hamilton Sundstrand. Because of electrified pneumatic systems and bleed manifold, the *HB-86* will utilize an electrical system that his a voltage system as shown in Table 10.3:

Table 10.3: Traditional/Untraditional Voltage Systems

Traditional	115 VAC / 28 VDC
Untraditional (No-bleed electrical architecture)	235 VAC / ±270 VDC

The system includes six generators (two per engine and two per APU) operating at 235 VAC. The generators are directly connected to the engine gearboxes and operate at a variable frequency (360 to 800 hertz) proportional to the engine speed. The HB-86 also has four, two forward and two aft, external power receptacles.

The backup system is powered by a Hamilton Sundstrand APS 5000. The APS 5000 APU is rated at 1,100 shaft horsepower and is designed to start and operate throughout the full range of the *HB-86*. The APS 5000 is capable of producing 1.450 MW of electrical power. Figure 10.4 displays the electrical layout:

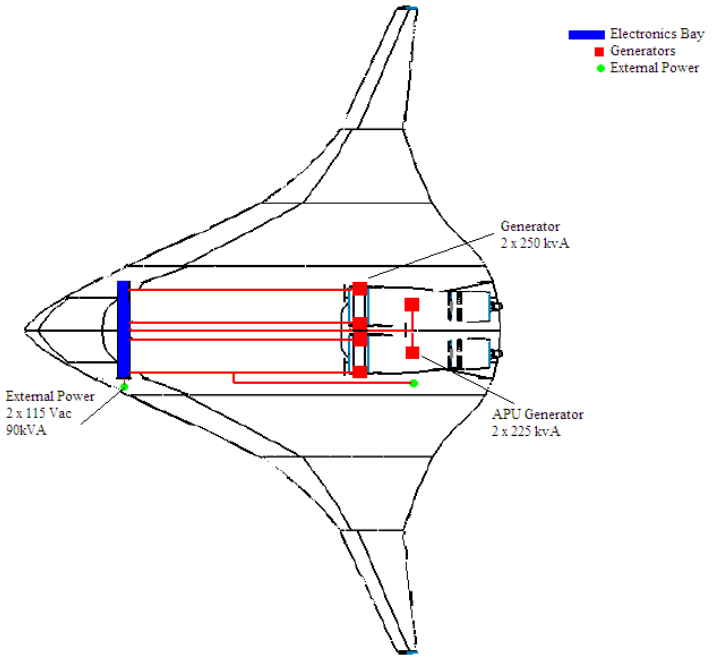

Figure 10.3: Electrical System Layout

10.4 Environmental Control Systems/Lavatories & Galleys

For cargo heating & air conditioning, products from Hamilton Sundstrand were chosen. The air management system will ventilate heat, cool, humidify, and pressurize the aircraft. Currently most commercial aircraft are pressurized at 8,000 ft. However, pressurizing the cabin at 6,000 ft and having humidity levels between 15 percent and 20 percent have been shown to reduce jet lag. The reduced pressure gives passengers more comfort and relaxation. The *HB-86* is currently pressurized at 8,000 ft. A revamped structural layout on future models will make it is possible to pressurize the cabin at 6,000 ft.

There are three lavatories located in the cabin with two in the economy section and one first class. Jamco[33] products are used for the lavatories as well as its interior sections. A single-action, time-delay, hand-free, infrared faucet makes washing easier (Figure 10.5). Plastic mirrors also make the lavatories appear more spacious and inviting without the penalty of weight (Figure 10.6).

Figure 10.4: Infared Faucet[33]

Figure 10.5: Lavatory Mirrors[33]

10.5 Anti-Icing and Lightning Protection Systems

Most previous anti-icing systems on aircraft rely on engine bleed air systems. An Ultra Electronics/GKN Aerospace[31] collaboration has led to an electro-thermal ice protection (Figure 10.7) system that does not use the conventional bleed air system. The system instead works by having electro-thermal mats attached to the control surfaces for de-icing measures. The electro-thermal mats are composed of multiple carbon and glass layers, each of

which are sprayed with a conductive metal acting as a heating element. The mats consume electricity form a range of 45-75 kW and operate at a temperature range of 45-70°F.

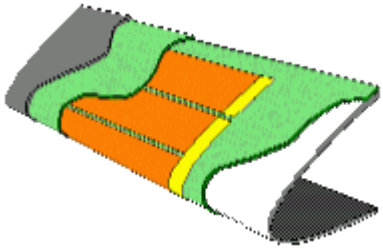

Figure 10.6: Electro-Thermal Mats in Wings[34]

The aircraft material will primarily serve as the lighting protection mechanism. Insurance of minimal gap in the surface will force any lighting current to remain on the exterior due to the conductive aluminum skin. Static wicks on the trailing edges will also aide in electricity dissipation.

10.6 Avionics

The avionics suite was selected based on the current Honeywell and Rockwell Collins products. One of the key technologies provided by Rockwell Collins[33] is a Heads-Up Guidance System (HGS). Originally used in combat aircraft, but the HGS has grown to a unique system that enhances situational awareness. Huge LCD screens (9”x12”) display layers of terrain data, radar, weather, and GPS all on one screen. The HGS projects primary flight guidance information onto a transparent glass screen directly into the pilot’s line of sight (Figure 10.8 on the following page). Rockwell Collins was also selected to supply the display control panels, multifunction keypads, and cursor control devices.

Figure 10.7: Heads-Up Guidance Display[35]

Figure 10.9 shows the cockpit on a Boeing 787[31]. The *HB-86* will have very similar layout due to the analogous relationship between the systems of the B787 and *Navigator*. Figure 10.10 displays a rendering of our cockpit. In Figure 10.10, the following indicate various components: 1) Heads-up guidance display, 2) Primary flight instrument display, 3) Navigation/Weather display, 4) Engine display, 5) Rudder pedals, 6) Autopilot, lighting controls, backup heading, artificial horizon and altimeter.

Figure 10.8: Boeing 787 Cockpit Layout[31]

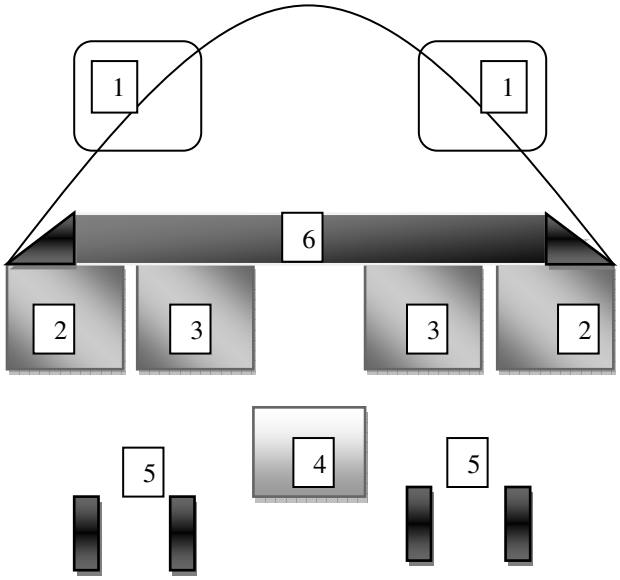

Figure 10.9: *Navigator* Cockpit Layout

10.7 In-Flight Entertainment System

The structural design of the *Navigator* prevents the installation of windows. There is a possibility of window installation in the first class section; however, the center seating in first class limits efficient views. To contour this, all seats will be fitted with small televisions screens for in-flight-entertainment. Another option for passengers will be to view what is going out outside the aircraft through externally mounted cameras on the sides and underbelly of the aircraft. Figure 10.11 displays a visual of the system:

Figure 10.10: In Flight Entertainment System[36]

10.8 Passenger/Cargo Loading

Figure 10.12 displays an isometric view of the *HB-86*. The red arrow displays the location for passenger loading, whereas the green points towards the location for cargo loading:

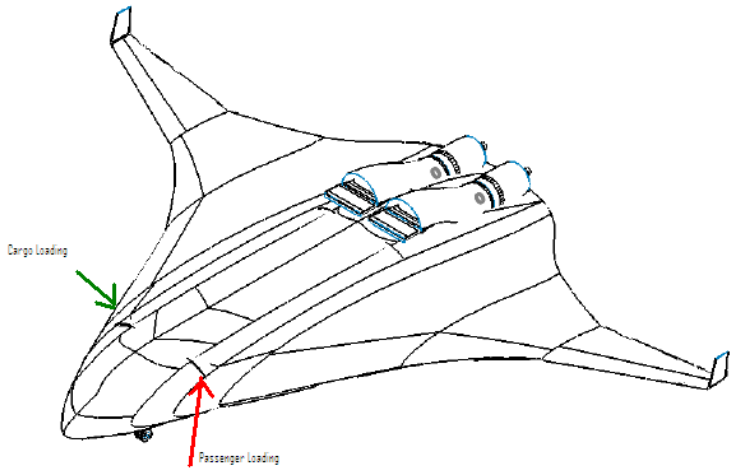

Figure 10.11: Locations of Passenger and Cargo Loading

Directly opposite the passenger door on the lower half of the aircraft, there is a cargo loading door present. Cargo is loaded onto containers (Model # - LD3-45) and sent up a ramp into the cargo section of the aircraft. Once the container reaches the inside of the *HB-86*, there are automated rollers on the floor controlled via a control panel. The rollers then move the containers to the rear of the aircraft for security and retention. Figure 10.13 shows a diagram of the cargo system:

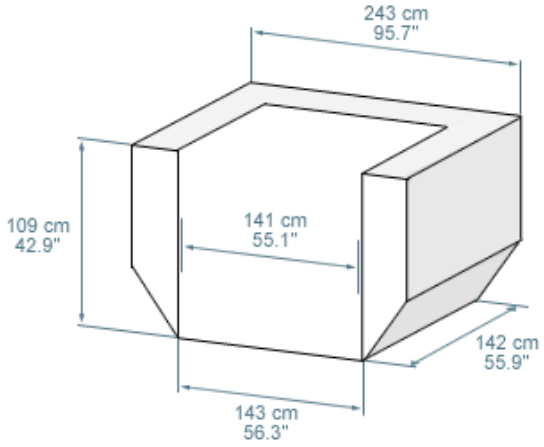

Figure 10.12: Cargo Layout

11. Cost Analysis

11.1 Introduction to Cost Analysis

The RFP states that flyway cost and life cycle cost are to be estimated with productions of 150, 500 and 1500 units. The cost modal for this report was acquired from Roskam[37]. Through this method, the Life Cycle Cost (LCC) of an airplane is divided into four categories:

- Cost of research, development, technology and evaluation (C_{RDTE})
- Cost of manufacturing and acquisition (C_{ACQ})
- Cost of operations (C_{OPS})
- Cost of Disposal (C_{DISP})

The summation of these four cost components will yield the LCC. For acquisition cost, the manufacturing cost (C_{MAN}) and the profit (C_{PRO}) must be summed to find the C_{ACQ}.

11.2 Initial Data

Data must first be initialized before executing our cost analysis algorithm. These includes the takeoff weight of the airplane (W_{TO}), the cruise speed (V_{max}), factor of difficulty (F_{diff}) which accounts for the difficulty of the design and manufacturability, factor of CAD designing (F_{CAD}) and Factor of Materials (F_{Mat}) which will take into account the different materials used on an airplane. Another factor for consideration is inflation; this can be offset by a value called the Cost Escalation Factor (CEF) which can be found through the consumer price index. When a cost of an airplane needs to be offset by inflation the following formula can be used:

$$COST_{present} = COST_{past}\left(\frac{CEF_{present}}{CEF_{past}}\right) \qquad \text{(Equation 11.1)}$$

For an example of the CEF over time, Figure 11.1 plots CEF values from 1989 to 2008:

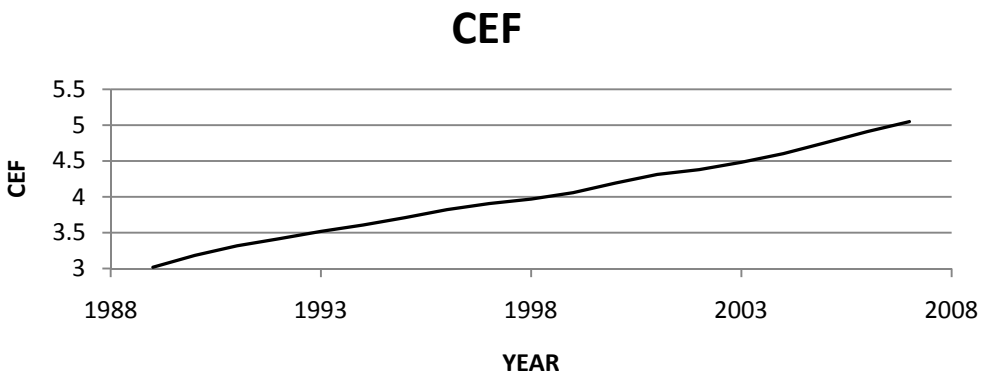

Figure 11.1: CEF Values from 1989 to 2008

The factors and properties that are going to be used in the hybrid wing cost analysis and, for comparison, the Boeing 737-500 are summarized in Table 11.1 below:

Table 11.1: Cost Factor Summary

	BWB	Boeing 737
W_{to}/lb	145000	154000
V_{max}/ kn	285	285
F_{diff}	2	2
F_{cad}	0.8	.8
F_{mat}	2.5	1
CEF_{2008}	5.04	5.04
CEF_{1989}	3.02	3.02

11.3 Cost of Research, Development, Technology and Evaluation

To determine the cost for research, development, technology, and evaluation, the following factors serve as components of the summation:

- The Airframe Engineering and Design Cost (C_{aed_r})
- Development Support and Testing Cost (C_{dst_r})
- Airplanes for Flight Testing Cost (C_{fta_r})
- Flight Testing Operating Cost (C_{fto_r})
- Test and Simulation Facilities Cost (C_{tsf_r})
- RDTE Profit (C_{pro_r})
- Cost to Finance RDTE (C_{fin_r})

Based upon our initial values, Table 11.2 shows a break-down and total of the several components:

Table 11.2: Break-Down of Research Cost

Cost Component	HB-86	Boeing 737-300
C_{aedr}	$205	$535
C_{dstr}	$57	$60
C_{ftor}	$48	$51
C_{ftar}	$980	$1,019
C_{pror}	$161	$196
C_{finr}	$161	$196
Total C_{rdte}	**$1,615**	**$1,969**

11.4 Acquisition Cost

The program acquisition cost will be found by determining the cost of manufacturing and the profit. Let's first take a look at C_{MAN} which can be broken down into 4 sub-groups as follows:

- Airframe engineering cost (C_{aed_m})
- Airplane production cost (C_{apc_m})
- Production flight test operation cost (C_{fto_m})
- Cost of financing the manufacturing program (C_{fin_m})

As the RFP requires the acquisition cost will be using 150, 500 and 1500 production units as part of the acquisition cost analysis. Along with our design there will be an acquisition cost analysis with the Boeing 737-300. Table 11.3 displays the results of the cost model analysis:

Table 11.3. Acquisition Cost

(cost shown in Millions)			
Cost category	150 units	500 units	1500 units
C_{aedm}	$145	$229	$325
C_{apcm}	$4,643	$10,812	$23,928
C_{ftom}	$38	$128	$384
C_{finm}	$965	$2,234	$4,927
C_{man}	$5,362	$12,411	$27,376
C_{pro}	$965	$2,234	$4,927
$C_{acq\_Navigator}$	**$6,328**	**$14,645**	**$32,303**
C_{acq_B737}	**$7,300**	**$16,624**	**$36,174**

11.5 Flyaway Cost

This section is to show the unit cost of each airplane for a production run of 150, 500 and 1500 units. This is determined by adding the C_{RDTE} and C_{ACQ}, then dividing it by the number of units. Table 11.4 displays the flyaway cost, while comparing to the Boeing-737:

Table 11.4: Flyaway Cost in Millions

Cost category	150 units	500 units	1500 units
C_{rdte}	$1,615	$1,615	$1,615
C_{acq}	$6,328	$14,645	$32,303
CEF(2009)	5.04	5.04	5.04
CEF(1989)	3.02	3.02	3.02
Flyaway cost (*Navigator*)	**$88**	**$54**	**$38**
Flyaway cost (B737)	$103	$62	$42

11.6 Operating Cost

When dealing with operating cost there are many factors that are usually kept constant for all airplanes like insurance cost, crew cost, etc., but in the case of our design a lower weight and a lower fuel burn this will account for the difference in operating cost from the Boeing 737-300. The table below summarizes the cost break down for the operating cost of both models:

Table 11.5: Operating Cost in Billions Breakdown (*Navigator*)

Cost category	150	500	1500
Nyr (number of operating years)	10	10	10
Rblann (distance travelled annually)/nm	758974	758974	758974
DOC (direct operating cost)/ ($/(yr*nm))	10.4	14.86	32.75
IOC (indirect operating cost) /($/(yr*nm))	8.32	11.88	26.2
Operating Cost (*Navigator*)	**$26**	**$89**	**$264**
Operating Cost (B737)	$28	$95	$287
Percent Difference	7%	6%	8%

As viewed above, our design has approximately an eight percent lower operating cost then the Boeing 737-300.

12 Conclusion

Justified by the proposed analysis, it can be seen that the *HB-86* satisfies, and often exceeds, the requirements in the AIAA RFP. The blending of the wing with the fuselage results in a significant advancement in aerodynamic configuration and performance. The inherent stability of the design allows the avoidance of heavy-drag inducing control surfaces (vertical tail, horizontal tail, etc.) The submerged propulsion inlet allows for smooth boundary layer control into the intake of a highly-advanced propulsion system. The *HB-86* satisfies the mission requirements of the RFP with high performance. Adaptability and flexibility in the design allows for smooth transition between takeoff, cruise, and landing. The following table lists significant requirements in the RFP, the compliance of the *Navigator*, and a section reference for justification:

Table 12.1: RFP Compliance

Parameters	Compliant?	Reference
Capacity: 150 seats, dual class.	Yes	Section 2
Cargo Capacity: > 7.5 ft^3/PAX	Yes (11.0 ft^3/PAX)	Section 10
Maximum Range: 2800 nm	Yes (2873 nm)	Section 6
Initial Cruise Altitude: 35,000 ft	Yes (38,000 ft)	Section 6
Community Noise	Yes	Section 5
Fuel Burn: 41 lbs/seat	Yes (41 lbs/seat)	Section 6
Operating Cost: 8% reduction	Yes	Section 11
Acquisition Cost: Commensurate	Yes	Section 11

REFERENCES

1. "2008-2009 AIAA Foundation Undergraduate Team Aircraft Design Team Competition." http://www.aoe.vt.edu/aoe/faculty/Mason_f/AIAA0809UgradTeamAirRFP.doc.

2. Jackson, Paul, *Jane's All the World's Aircraft*, Sampson Low, Marston & Co, London, 2008.

3. Student Presentation, *Three Surface*, www.aoe.vt.edu/~mason/Mason_f/ThreeSurfaceS04.ppt

4. Liebeck, R, "Design of the Blended Wing Body Subsonic Transport," AIAA-2002-0002, 2004.

5. Roman, D., and Allen, JB, "Aerodynamic Design Challenges of the Blended-Wing Body Subsonic Transport," AIAA 2000-4335.

6. Raymer, Daniel P, *Aircraft Design: A Conceptual Approach*, 4th ed, AIAA, Reston, VA, 2006.

7. Mason, William H., AOE 4065-4066 Design (Aircraft), 2008-2009, http://www.aoe.vt.edu/~mason/Mason_f/SD1.html.

8. *Avro-Vulcan*. http://www.scribd.com/doc/512720/Avro-Vulcan.

9. Roskam, Jan, Airplane Design Part V, *Component Weight Estimation*, DAR corporation, Lawrence, KS, 2005.

10. *The Boeing 737 Technical Site*, http://www.b737.org.uk/.

11. "CFM56-7B Technology". 2009. CFM International. http://www.cfm56.com/products/cfm56-7b/9660

12. "V2500 Engine Facts". International Aero Engines. http://www.v2500.com/engine/data.shtml.

13. "PurePower PW1000G Characteristics". Pratt and Whitney. http://www.pw.utc.com/vgn-ext-templating/v/index.jsp?vgnextoid=59ab4d845c37a110VgnVCM100000c45a529fRCRD.

14. "Commercial Aero Engine Components". Volvo Aero Global. 2007, http://www.volvo.com/volvoaero/global/en-b/products/Engine+components/commercial_engines/commercial_engines.htm?TAB=15.

15. Leiffson, Leifur Thor. "Multidisciplinary Design Optimization of Low-Noise Transport Aircraft". Ph.D. Dissertation, Virginia Polytechnic Institute and State University. Blacksburg, VA. 2005.

16. Mason,Dr. William, H., "Transonic Aerodynamics of Airfoils and Wings," March 10, 2006, http://www.aoe.vt.edu/~mason/Mason_f/ConfigAeroTransonics.pdf.

17. "UIUC Airfoil Coordinates Database." http://www.ae.uiuc.edu/m-selig/ads/coord_database.html.

18. Wilby, P.G., "The Design and Aerodynamic Characteristics of the RAE 5215 Aerofoil," Aerodynamics Dept., RAE, Farnborough Hants, http://aerade.cranfield.ac.uk/ara/arc/cp/1386.pdf.

19. Stahara, S. S., "NASA-CR-3064," NASA, 1978.

20. Roskam, Dr. Jan, "Drag Polar Prediction Methods," *Airplane Design: Part VI: Preliminary Calculation of Aerodynamic, Thrust and Power Characteristics*, 5th ed., DARCorporation, Lawrence, Kansas, 2008, pp. 21-113.

21. Mason, Dr. William, H., "Friction.f", <http://www.aoe.vt.edu/~mason/Mason_f/SD1.html>.

22. Northrop, J.K. "The Development of All-Wing Aircraft," *The Royal Aeronautical Society*, Vol 51, 1947, pp.481-510.

23. Kay, J, et. al., "Control Authority Issues in Aircraft Conceptual Design: Critical Conditions, Estimation Methodology, Spreadsheet Assessment, Trim and Bibliography," Department of Aerospace and Ocean Engineering, VPI-Aero-200, 1996.

24. Waszak, Marty, "VIP-NASA-CPC", NASA Langley, http://www.aoe.vt.edu/~mason/Mason_f/SD1.html.

25. Niu, Michael Chun-Yung, *Airframe Structural Design*, Conmilit Press Ltd., 1988.

26. "The Airbus A380", http://www.airliners.net/aircraft-data/stats.main?id=29.

27. Baker, Alan, Dutton, Stuart, Donald, Kelly, *Composite Materials for Aircraft Structures*, 2nd Edition, AIAA Education Series, 2004.

28. "Vacuum Infusion of an Aircraft C-Spar; a Low Cost Alternative for Prepegging", http://www.lightweight-structures.com/index.php?option=com_content&task=view&id=33.

29. "Good Year Tire Data," http://www.goodyearaviation.com/resources/pdf/datatires.pdf.

30. "Electric Braking, a Major Technological Advance", http://www.messierbugatti.com/rubrique.php3?id_rubrique=57&lang=en.

31. "Hamilton Sundstrand Nearing Completion of Delivery of Systems for Boeing 787 Dreamliner" http://www.examiner.com/p-65~Hamilton_Sundstrand_Nearing_Completion_of_Delivery_of_Systems_for_Boeing_787_Dreamliner.html.

32. "787 No-Bleed Air Systems," http://www.boeing.com/commercial/aeromagazine/articles/qtr_4_07/article_02_4.html.

33. "JAMCO Aircraft Interiors," http://www.jamco.co.jp/e/e-interiors/e-lavatory/lav-index.html.

34. Wing Ice Protection," http://www.ultracontrols.aero/Products/Wips.htm.

35. "Heads Up Display," http://2.bp.blogspot.com/_diedsJj6wzM/STqjLYc4MPI/AAAAAAAADpk/6-29RNhNxUw/s400/hgs.jpg.

36. "Johnnyjet.com" http://www.johnnyjet.com/images/PicForNewsletterJapan2005JalInFlightEntertainemnt.JPG.

37. Roskam, Jan, Airplane Design Part VII, *Cost Estimation*, DAR corporation, 2005.

38. Norris, Thomas, Wagner, Forbes Smith. Boeing 787 *Dreamliner* – flying redefined. Aerospace Technical Publications International Pty Ltd., 2005.